Article

Not peer-reviewed version

Polylactic Acid/Polymethylsilsesquioxane (PLA/PMSQ) Microparticle Composites: Development and Characterization

Khadim Mboup *, Fouad Erchiqui, Denis Rodrigue, Karima Ben Hamou, Abdessamad Baatti

Posted Date: 22 May 2026

doi: 10.20944/preprints202605.1499.v1

Keywords: polylactic acid (PLA); polymethylsilsesquioxane (PMSQ); biocomposites; thermomechanical properties; rheological analysis

 doi:10.20944/preprints202605.1499.v1

Article

Polylactic Acid/Polymethylsilsesquioxane (PLA/PMSQ) Microparticle Composites: Development and Characterization

Khadim Mboup [1,*], Fouad Erchiqui [1], Denis Rodrigue [2], Karima Ben Hamou [3] and Abdessamad Baatti [1]

[1] Université du Québec en Abitibi-Témiscamingue, Rouyn-Noranda, QC, Canada
[2] Université Laval, Québec, QC, Canada
[3] Université de Moncton, Moncton, NB, Canada
* Correspondence: mbok01@uqat.ca

Abstract

This study presents the development of polylactide (PLA)-based biocomposites reinforced with 5, 10, and 15 wt.% polymethylsilsesquioxane (PMSQ) microparticles. The materials were prepared by melt blending followed by injection molding to evaluate the effect of PMSQ content on the morphological, thermal, mechanical, thermomechanical, rheological, and thermal conductivity properties of polylactic acid (PLA). Scanning electron microscopy (SEM) revealed a relatively uniform dispersion of PMSQ particles, especially at low filler content (up to 5 wt.%). Differential scanning calorimetry (DSC) showed that PMSQ incorporation did not significantly affect the melting temperature of PLA, while the cold crystallization temperature decreased by 14 °C combined with a higher crystallinity level. Thermogravimetric analysis (TGA) showed a slight improvement in thermal stability, with higher residual mass as PMSQ content increased. Mechanical tests showed a 7.4% reduction in Young's modulus and a 20% loss of tensile strength for the biocomposite containing 15 wt.% PMSQ due to limited interfacial stress transfer and particle agglomeration. However, dynamic mechanical analysis showed that low PMSQ concentration (5 wt.%) increased the storage modulus by 15% at 35 °C and slightly increased the glass transition temperature by up to 2 °C. Rheological analyses revealed higher storage modulus, loss modulus, and complex viscosity with increasing PMSQ content. Additionally, the presence of PMSQ enhanced the thermal conductivity of PLA by up to 23% at 75 °C. Overall, PLA/PMSQ biocomposites, especially at low PMSQ content, showed improved thermomechanical stability and thermal conductivity, suggesting their potential use in thermoforming applications.

Keywords: polylactic acid (PLA); polymethylsilsesquioxane (PMSQ); biocomposites; thermomechanical properties; rheological analysis

1. Introduction

The depletion of petroleum resources, increasing greenhouse gas (GHG) emissions, and accumulation of synthetic plastic waste represent major environmental challenges worldwide. These issues have intensified the search for sustainable alternatives to protect both the environment and human health (Silva et al., 2014). In this context, bioplastics have attracted increasing attention over the past decades in both academic and industrial sectors. Numerous studies investigated biopolymers as matrices, while their applications in packaging, engineering components, and biomedical devices are still expanding (Cristea et al., 2020; D'Anna et al., 2022; Kaynak and Meyva, 2014; Lecoublet et al., 2024; Rbihi et al., 2025).

Polylactide (PLA) is one of the most extensively used biopolymers due to its good mechanical and thermal properties, similar to those of conventional polymers such as polystyrene (PS) and

 doi:10.20944/preprints202605.1499.v1

polyethylene terephthalate (PET) (Kaynak and Erdogan, 2016; Swetha et al., 2023). In addition, PLA benefits from wide market availability (Neoh et al., 2011). Due to its biodegradability and biocompatibility, PLA is widely used in packaging and biomedical applications, in contrast to most petroleum-based polymers (Gupta and Kumar, 2007; Madhavan Nampoothiri et al., 2010). Despite these advantages, the use of PLA in demanding engineering applications remains limited by its drawbacks, including inherent brittleness and limited thermomechanical performance (Awal et al., 2015; Neoh et al., 2011).

Several strategies have been proposed to overcome the intrinsic limitations of PLA, including copolymerization (D'Anna et al., 2019; Jandas et al., 2014) and the incorporation of micro- or nano-fillers to produce biocomposites (Lee and Jeong, 2014). Filler incorporation is a widely used approach to improve the mechanical, thermomechanical, and thermal performance of PLA. Commonly investigated reinforcements include natural fibers (wood, kenaf, sisal), mineral fillers (calcium carbonate, calcium sulfate, clay, silica), and carbon-based materials (carbon nanotubes, graphite, graphene, carbon black) (Can and Kaynak, 2020). However, these fillers often show limited interfacial compatibility with the polymer matrix, which usually requires the use of coupling agents or surface treatments to improve filler–matrix adhesion.

Coupling agents, such as maleic anhydride-grafted polypropylene (MAPP), maleic anhydride-grafted polyethylene (MAPE), and maleic anhydride-grafted polylactide (MAPLA), are widely used to enhance interfacial interactions in polymer composites (Rao et al., 2018). Due to their dual hydrophilic–hydrophobic character, these compatibilizers promote matrix-filler interactions, resulting in enhanced mechanical and physical performance (Kim et al., 2011). In this study, MAPP was used as a coupling agent to improve the interfacial interactions in the PLA/PMSQ system. Its selection was based on the assumed affinity between the hydrophobic PP backbone and PMSQ combined with potential interactions between the maleic anhydride groups and PLA.

Hybrid reinforcements, such as polyhedral oligomeric silsesquioxanes (POSS), have been reported in the literature. Sirin et al. investigated the effect of POSS particles functionalized with amine, hydroxyl, and epoxy groups on PLA properties (Sirin et al., 2016). These additives acted as processing aids by decreasing the viscosity, while simultaneously enhancing mechanical properties, such as impact strength and the elongation at break. Adding hydroxyl-functionalized POSS (T-POSS) led to a 18% increase in elongation at break. However, all formulations exhibited lower Young's modulus and yield strength, which was attributed to particle agglomeration.

Similar to POSS, polymethylsilsesquioxane (PMSQ) microparticles belong to the silsesquioxane family. They are typically synthesized via a two-step sol–gel process and exhibit a hybrid organic–inorganic structure. Their general chemical formula is $RSiO_{1.5}$, where R may be hydrogen or organic substituents such as phenyl, methyl, or vinyl groups (Yao et al., 2018). PMSQ shares several characteristics with silica, including high thermal and chemical stability, as well as good flame-retardant performance (Donmez et al., 2024; Meng et al., 2021). In addition, the presence of methyl groups imparts hydrophobic behavior (Chang et al., 2025). Because of this combination of structural rigidity, thermal stability, and surface characteristics, PMSQ microparticles represent a promising reinforcement to improve the performance of thermoplastic matrices and their application potential.

Although PLA-based biocomposites have been widely investigated, the incorporation of PMSQ microparticles in PLA remains scarce. Recently, Anjrini et al. developed 3D-printed PLA/PMSQ scaffolds for biomedical applications using low PMSQ contents (1-2 wt.%) (Anjrini et al., 2024). The structures were fabricated via extrusion-based bioprinting and subsequently coated with vitamin E microparticles. Their results revealed a 26% decrease in tensile strength at 2 wt.% PMSQ. However, the thermomechanical and rheological behavior of PLA/PMSQ biocomposites were not evaluated, thereby limiting the understanding of their performance under conventional melt-processing conditions. Consequently, the structure–property relationships governing PLA/PMSQ systems remain poorly understood.

PLA is inherently brittle and exhibits limited thermal and thermomechanical stability, which restrict its use in demanding applications such as thermoforming. In addition, its low thermal

 doi:10.20944/preprints202605.1499.v1

conductivity may result in longer heating times. Therefore, improving the thermal stability, thermomechanical behavior, and thermal conductivity of PLA remains a significant challenge from both academic and industrial perspectives. In this context, the incorporation of PMSQ microparticles emerges as a promising strategy to address these limitations.

The objective of this work is to evaluate the effect of PMSQ microparticles on the properties of PLA, with a focus on thermal, mechanical, and thermomechanical properties, as well as rheological behavior and thermal conductivity. To the best of our knowledge, no previous study has comprehensively investigated PLA/PMSQ biocomposites produced via conventional melt processing while simultaneously evaluating several important properties. The originality of this study lies in the development of PLA/PMSQ biocomposites through extrusion, with an approach designed to simultaneously assess their main properties for possible applications in thermoforming.

2. Materials and Methods

2.1. Materials

The polylactide (PLA) used in this study was an injection-grade resin (PLI005), with a melt flow index (MFI) of 25–35 g/10 min (2.16 kg, 190 °C) and a density of 1.25 g/cm^3, supplied by NaturePlast (France). Polymethylsilsesquioxane (PMSQ) was provided by Guangzhou Batai New Material Technology Co. Ltd. (China) as spherical microparticles in the form of a white powder. Maleic anhydride-grafted polypropylene (MAPP) was supplied in a granular form by Sigma-Aldrich (USA). This grade has a density of 0.934 g/mL at 25 °C and a melting temperature of 156 °C.

2.2. Composites Manufacturing Process

Figure 1 outlines the composite preparation procedure and **Table 1** summarizes the prepared formulations. PLA and MAPP were first oven-dried at 60 °C for 8 h prior to processing. The compounds were prepared using a Haake PolyLab co-rotating twin-screw extruder (diameter = 24 mm; L/D ratio = 40) operated at a screw speed of 50 rpm and a temperature profile of 170/175/175/165 °C. The extrudates were pelletized and dried again at 60 °C for 8 h. The specimens were subsequently produced by injection molding using a PN60 injection molding machine (Nissei, Japan). The nozzle/front/middle/rear barrel temperatures were set at 180/185/180/175 °C respectively, and the mold temperature was maintained at 35 °C.

Table 1. Biocomposites formulations.

Sample	PLA (wt.%)	PMSQ (wt.%)	MAPP (wt.%)
PLA	100	0	0
PLA+5%PMSQ	92	5	3
PLA+10%PMSQ	87	10	3
PLA+15%PMSQ	82	15	3

 doi:10.20944/preprints202605.1499.v1

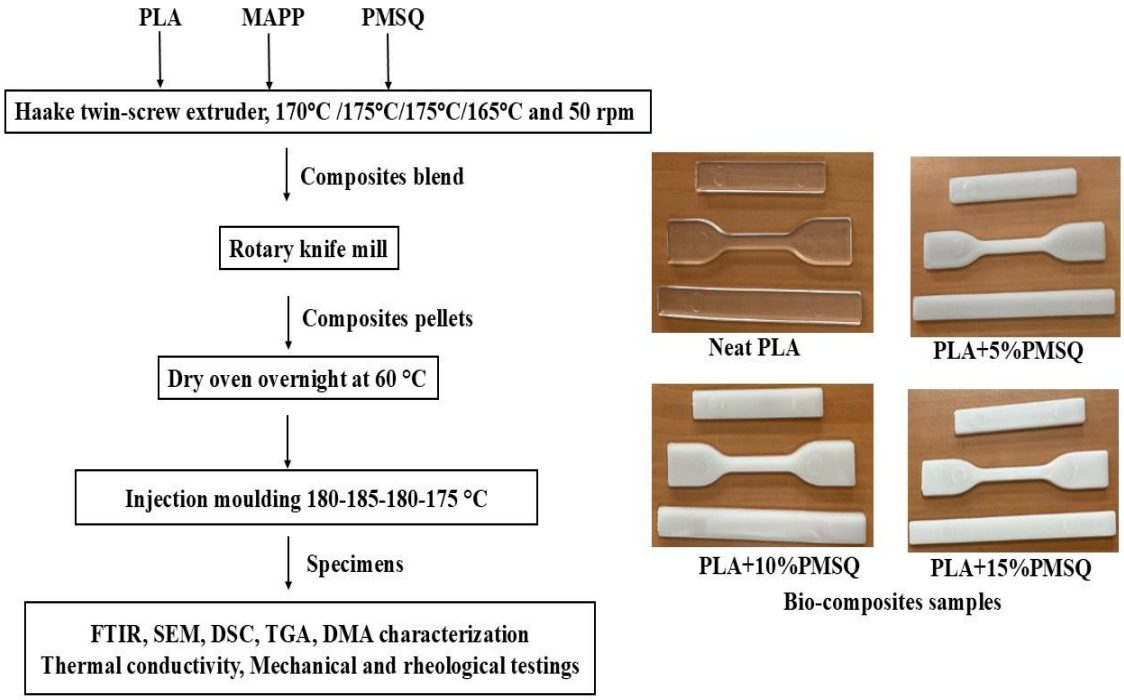

Figure 1. Schematic illustration of the PLA/PMSQ biocomposites preparation steps (extrusion compounding and injection molding).

2.3. Characterization

Infrared spectra were recorded using Fourier transform infrared spectroscopy (FTIR) in transmittance mode with a resolution of 8 cm^{-1} and 64 scans over the range of 4000–400 cm^{-1} at room temperature. The analyses were conducted on samples measuring 1 cm × 2 cm using a Shimadzu IR Tracer-100 spectrometer (Japan).

Morphological characterization was carried out using a JEOL JSM-840 scanning electron microscope (SEM) (Japan) operated at an accelerating voltage of 15 kV. The fracture surfaces were sputter-coated with gold prior to observation.

Differential scanning calorimetry (DSC) was conducted to determine the melting temperature (T_m), glass transition temperature (T_g), melting enthalpy (ΔH_m), crystallization enthalpy (ΔH_c), and degree of crystallinity (χ_c) of the composites. The measurements were performed using a Q20 calorimeter (TA Instruments, USA). Samples around 15 mg were heated from 20 to 220 °C under a nitrogen flow of 10 mL/min. To erase the thermal history, an isothermal step was applied at 220 °C for 1 min. The samples were subsequently cooled to 20 °C and reheated under identical conditions. The degree of crystallinity (χ_c) was calculated from the second heating cycle using the following equation (Fischer et al., 1973):

$$\boldsymbol{\chi_c}(\%) = \frac{\boldsymbol{\Delta H_m - \Delta Hc}}{\boldsymbol{(1-w)\,\Delta H^{\circ}_{100}}}\ \boldsymbol{(100)}\ \boldsymbol{(Equation\ 1)}$$

where ΔH°_{100} (93 J/g) represents the melting enthalpy of 100% crystalline PLA and w is the filler weight fraction (Aliotta et al., 2019; Yu et al., 2012).

Thermogravimetric analysis (TGA) was performed using a Q50 analyzer (TA Instruments, USA) to evaluate the thermal degradation behavior of the composites. Samples (around 20 mg) were heated from 25 to 600 °C at a heating rate of 10 °C/min under a nitrogen atmosphere.

Tensile tests were performed at ambient temperature following ASTM D638 using an Instron 5565 universal testing machine (Instron, USA) equipped with a 500 N load cell and a crosshead speed of 5 mm/min. For each formulation, five type IV specimens with a thickness of 3 mm were tested. The

 doi:10.20944/preprints202605.1499.v1

average values of tensile strength (Rp), yield strength (Rm), tensile modulus (E), yield strain (ε_m) and elongation at break (ε_r) were calculated together with their standard deviations.

Impact resistance (Charpy) was evaluated using an Impact 104 pendulum tester (Tinius Olsen, USA) following ASTM D6110. For each formulation, at least ten rectangular specimens (60 mm × 12.7 mm × 3.1 mm) were tested.

Dynamic mechanical analysis (DMA) was carried out using a RSA 3 analyzer (TA Instruments, USA). Temperature sweeps were performed from 30 to 140 °C at a heating rate of 1 °C/min, with a fixed frequency of 1 Hz and a strain amplitude of 0.005%. Rectangular specimens (3 mm × 12.7 mm × 50 mm) were tested in three-point bending mode using a span length of 40 mm.

Rheological measurements were carried out using an oscillatory disk rheometer (ARES, TA Instruments, USA) using small amplitude oscillatory shear (SAOS). The samples were compression molded into circular disks with a diameter of 25 mm and a thickness of 2 mm. Strain sweep tests were first conducted at 180 °C to determine the linear viscoelastic (LVE) region. Subsequently, frequency sweep tests were performed within the LVE regime at a fixed strain of 30% over an angular frequency range of 0.01–80 rad/s using a gap distance of 1.5 mm.

Thermal conductivity (k) measurements were performed using a custom-built apparatus based on ASTM E1225. Square specimens (50 mm × 50 mm) with an average thickness (L) of 3 mm were tested. The setup consisted of an upper and lower plate maintained at 33 °C and 13 °C respectively, generating a temperature difference (ΔT) of 20 °C with an average temperature of 23 °C (ambient conditions). But other temperatures were investigated to determine its effect on k. Each specimen was placed between thin aluminum foils to minimize interfacial thermal resistance and subjected to a compressive load of 7.2 kg to ensure proper thermal contact. The thermal conductivity (k) was calculated using Fourier's law as (Tong, 2011):

$$\mathbf{k} = \frac{Q\,L}{A\,\Delta T} \quad \textbf{(Equation 2)}$$

where Q is the heat transfer rate (W), L is the specimen thickness (m), A is the cross-sectional area (m^2), and ΔT is the applied temperature difference (K).

3. Results and Discussion

3.1. Fourier Transform Infrared Spectroscopy (FTIR)

Figure 2 presents the chemical structures of the materials used (PLA, PMSQ, and MAPP). This helps to understand the spectra for analyses, the functional groups present and possible interactions between them.

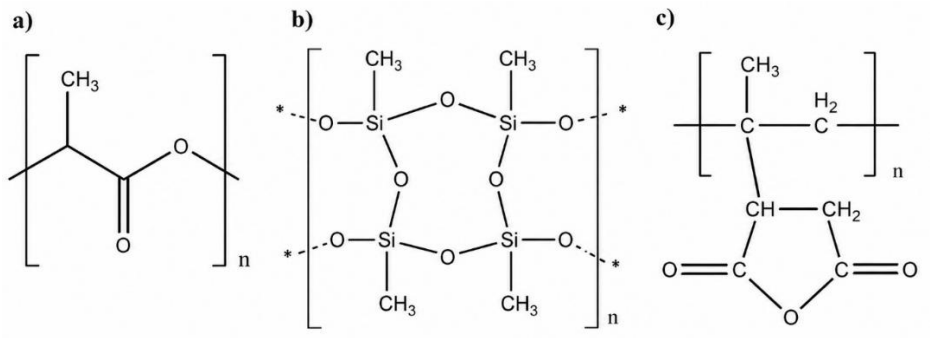

Figure 2. Chemical structures of the materials used: a) PLA, b) PMSQ, and c) MAPP.

Figure 3 presents the FTIR spectra of neat PLA, PMSQ powder, and the corresponding biocomposites. The spectra show the characteristic absorption bands of PLA (**Figure 3a**): the asymmetric and symmetric C–H stretching vibrations of methyl groups and backbone appear at 2993 and 2939 cm^{-1}, respectively (Wen et al., 2009). A strong absorption band at 1747 cm^{-1} is attributed to the C=O stretching vibration of the ester functional group. Bands at 1454, 1380, and 1360 cm^{-1} correspond to the asymmetric and symmetric deformation modes of CH_3 groups. In addition, the

 doi:10.20944/preprints202605.1499.v1

peaks at 1180 and 1081 cm^{-1} are assigned to the asymmetric and symmetric stretching vibrations of C–O–C linkages in the PLA structure (Moliner et al., 2020).

The FTIR spectrum of PMSQ (**Figure 3a**) exhibits a characteristic band at 2974 cm^{-1} corresponding to the asymmetric C–H stretching vibration of methyl groups. The peak at 1271 cm^{-1} is assigned to Si–CH_3 vibrations, while the asymmetric and symmetric stretching modes of the Si–O–Si bond are observed at 1100 and 1002 cm^{-1}, respectively. Additionally, bands at 852 and 763 cm^{-1} are attributed to the out-of-plane deformation vibrations of Si–CH_3 groups (Oseh et al., 2019; Yao et al., 2018).

In the PMSQ characteristic region (1400–600 cm^{-1}, **Figure 3b**), the asymmetric and symmetric Si–O–Si stretching vibrations at 1100 and 1002 cm^{-1} partially overlap with the C–O–C stretching bands of PLA located at 1180 and 1081 cm^{-1}. Nevertheless, the peaks at 1271 and 763 cm^{-1} can serve as clear indicators of PMSQ inside PLA. As shown in **Figure 3b**, neat PLA does not display a band at 1271 cm^{-1}, which is associated with Si–CH_3 vibrations in PMSQ. With increasing PMSQ content, this band becomes progressively more intense, a confirmation of the presence and increasing concentration of the filler. Moreover, the out-of-plane Si–CH_3 vibration, initially observed at 763 cm^{-1} in neat PMSQ, shifts toward higher wavenumbers (784 cm^{-1}) in the biocomposites, coupled with an intensity increase. In addition, the C=O absorption band at 1747 cm^{-1} becomes more pronounced in the biocomposites, which can be attributed to the incorporation of MAPP, containing carbonyl functional groups in its structure.

Overall, these spectral features confirm the successful incorporation of PMSQ inside the PLA matrix and suggest the contribution of MAPP to interfacial interactions.

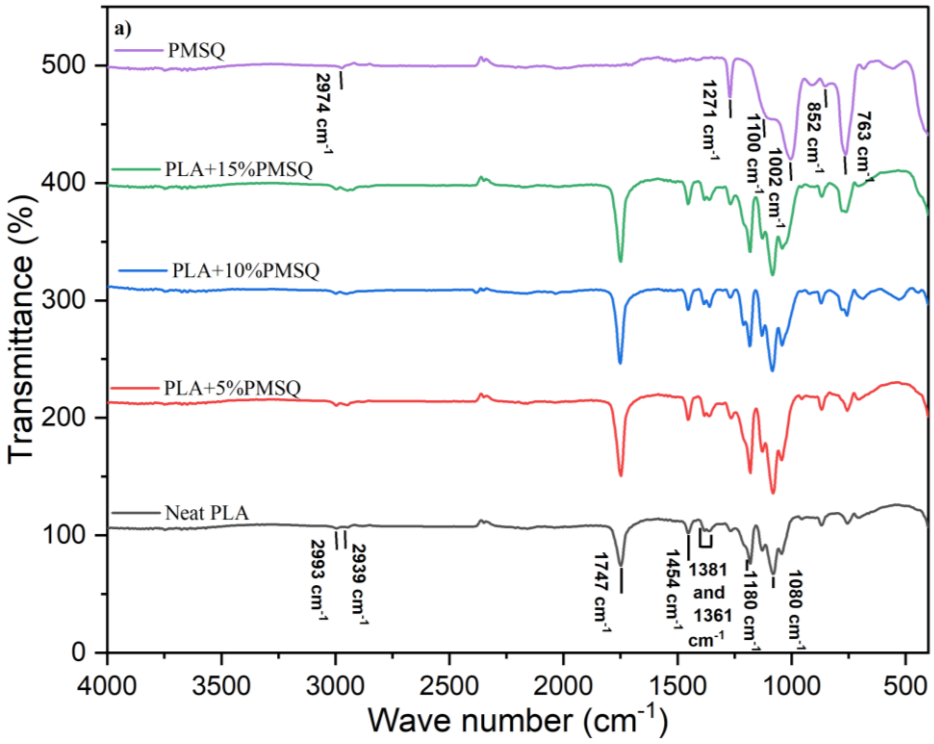

 doi:10.20944/preprints202605.1499.v1

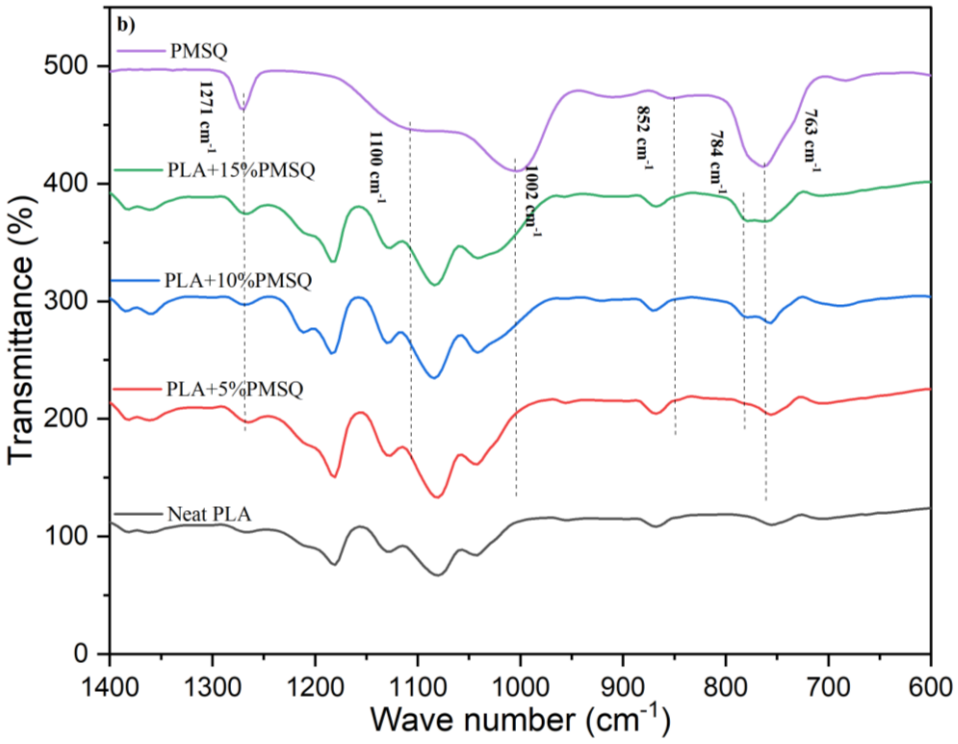

Figure 3. Infrared spectra of: a) neat PLA, PMSQ powder, and PLA/PMSQ biocomposites; b) Magnification of the spectra for the range 1400-600 cm^{-1}.

3.2. Scanning Electron Microscopy (SEM)

Figure 4 presents typical SEM micrographs of the neat PLA and PLA/PMSQ biocomposites.

The coated surface of neat PLA appears smooth and relatively flat, which is typical of a brittle fracture behavior (Jia et al., 2019). In contrast, the biocomposites exhibit markedly rougher fracture surfaces, indicating structural modifications induced by filler incorporation. This increased surface texture suggests changes in the internal morphology of the matrix, potentially associated with variations in crystallinity, as discussed later (Lecoublet et al., 2024). Moreover, the PMSQ particles retain their spherical morphology (rigid filler) after processing, with a fraction of the particles clearly embedded within the PLA matrix.

The SEM micrograph of PLA+5%PMSQ reveals a relatively uniform particle dispersion without agglomeration. This may be attributed to the presence of MAPP, which improved the dispersion of PMSQ particles inside the matrix. In contrast, the biocomposites containing 10 and 15 wt.% PMSQ display localized particle clusters, indicating that higher filler content compromises dispersion. This microstructural difference suggests that the composite containing 5 wt.% PMSQ may exhibit enhanced mechanical and thermomechanical performance, as discussed in subsequent sections.

An increase in PMSQ content also results in a higher particle density throughout the matrix. Compared to neat PLA, the biocomposites have some pores, especially at higher filler content. These cavities are likely associated with particle debonding or pull-out during fracture. Such defects are commonly attributed to insufficient interfacial adhesion between the polymer matrix and the filler (Jiang et al., 2007).

 doi:10.20944/preprints202605.1499.v1

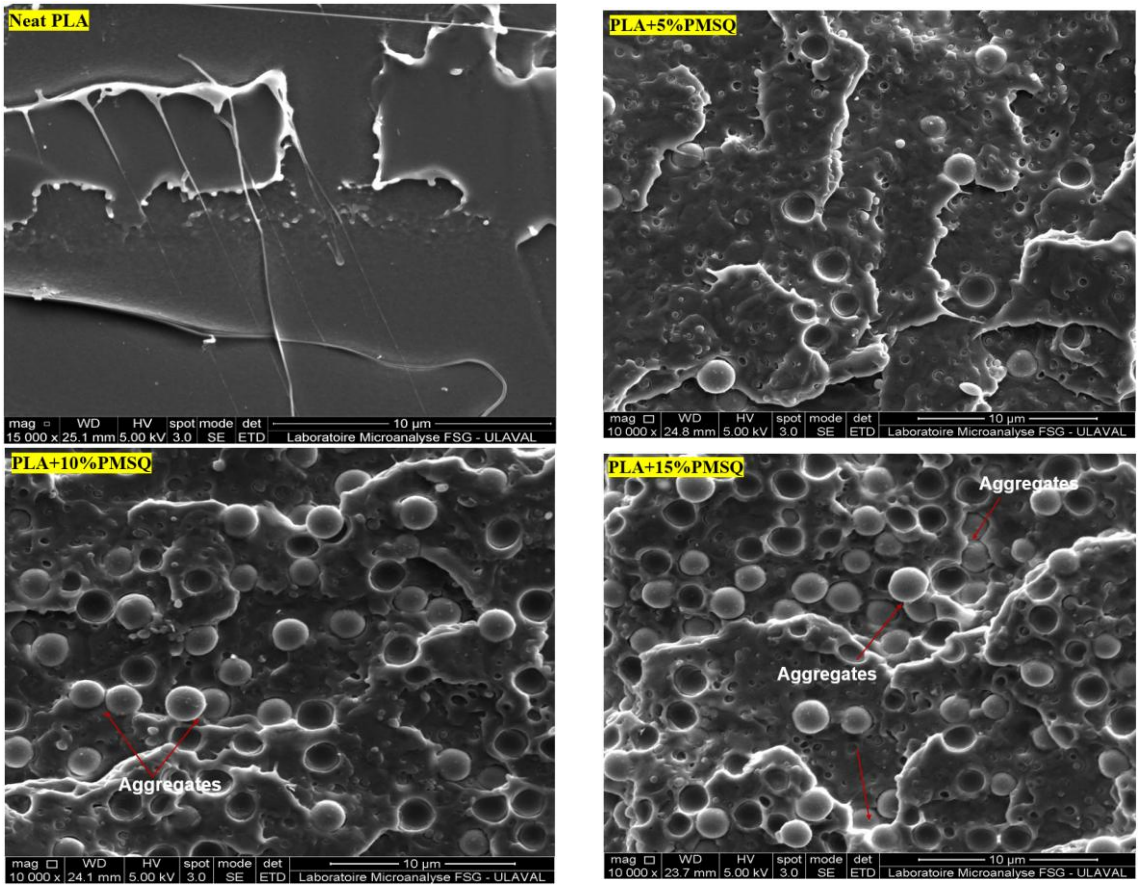

Figure 4. SEM images of neat PLA and PLA/PMSQ biocomposites.

3.3. Thermal Analyses

Figure 5 presents the DSC thermograms obtained during the second heating cycle, and the corresponding thermal parameters are summarized in **Table 2**. The results indicate that the incorporation of PMSQ microparticles does not significantly affect either the glass transition temperature (T_g) or the melting temperature (T_m) of PLA. This suggests that the overall crystalline structure of PLA remains largely unchanged after filler incorporation. PMSQ addition does not appear to alter the free volume nor induce the formation of imperfect crystalline structures that could lower the melting temperature. Similar results were reported for PLA reinforced with POSS particles (Sirin et al., 2016). In contrast, Yu et al. observed an increase in T_g upon the addition of talc microparticles, which was attributed to strong interfacial interactions restricting polymer chain mobility and reducing free volume (Yu et al., 2012).

Table 2 further indicates that PMSQ incorporation significantly decreases the cold crystallization temperature (T_{cc}) of PLA by up to 14 °C, suggesting that PMSQ microparticles act as effective nucleating agents (Sirin et al., 2016). Similar trends have been reported in the literature. For example, Orisekeh et al. observed a reduction in T_{cc} from 122 °C to 92.5 °C following the incorporation of 5 wt.% eggshell microparticles into PLA (Orisekeh et al., 2025). The decrease in T_{cc} is coupled with a significant increase in the degree of crystallinity with increasing PMSQ content, another confirmation of the nucleating effect. The highest crystallinity is achieved at 5 wt.% PMSQ compared to neat PLA. However, a slight reduction in crystallinity is observed at higher filler concentrations. This behavior may indicate a nucleation saturation threshold around 5 wt.%, above which polymer chain confinement restricts further crystal growth (Soudmand et al., 2020). From a processing perspective, lower T_{cc} suggests that crystallization can occur at lower temperatures, potentially reducing the energy required during processing while promoting improved mechanical performance relative to neat PLA (Orisekeh et al., 2025; Silva et al., 2014).

 doi:10.20944/preprints202605.1499.v1

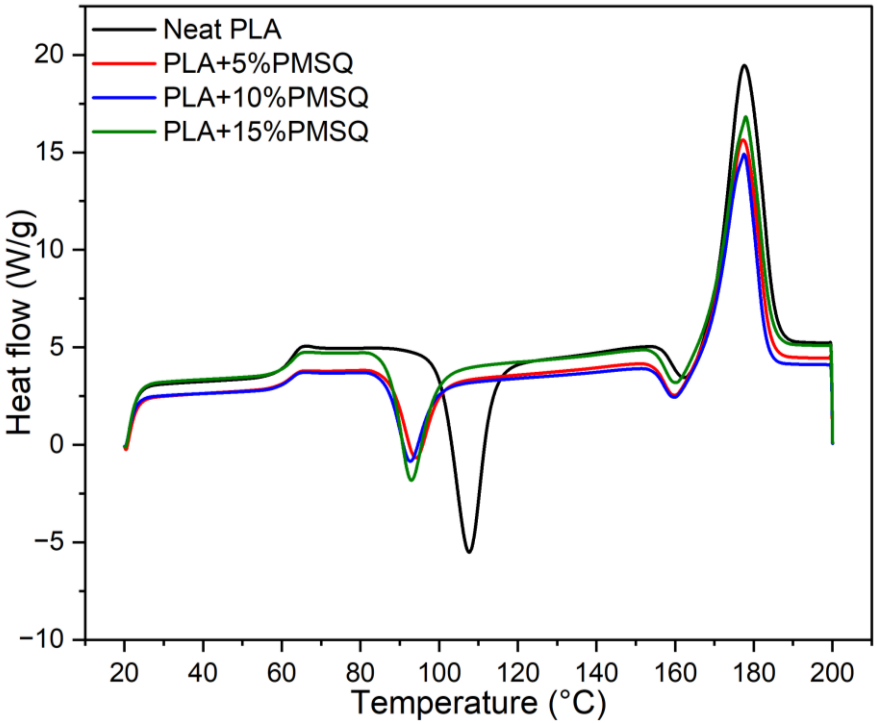

Figure 5. DSC curves of the neat PLA and PLA/PMSQ biocomposites.

Table 2. Summary of DSC and TGA thermal data for neat PLA and PLA/PMSQ biocomposites.

Sample	DSC data									TGA data	
	Melting process			Crystallization process							
	T_m (°C)	ΔH_m (J/g)	T_g (°C)	χ_c (%)	T_{cc} (°C)	ΔH_c (J/g)	$T_{5\%}$ (°C)	$T_{25\%}$ (°C)	$T_{50\%}$ (°C)	T_{max} (°C)	Residues at 600 °C (wt.%)
Neat PLA	177.6	45.8	65.5	16.1	107.7	30.1	344.2	363.7	374.5	378.9	4.46
PLA+5%PMSQ	177.3	43.6	65.1	32.9	94.2	16.1	345.8	365.8	377.1	381.1	7.01
PLA+10%PMSQ	177.6	41.0	64.9	28.1	92.6	17.4	342.2	364.0	375.7	380.9	8.00
PLA+15%PMSQ	177.9	38.1	65.4	25.3	93.0	18.1	342.1	365.1	377.5	380.1	14.72

The heat capacity (Cp) of neat PLA and PLA/PMSQ composites is presented in **Figure 6**. Heat capacity reflects the energy required to increase the temperature of a material by one degree and is closely related to the mobility of macromolecular chains (Guo and Shi, 2011; Pyda et al., 2004).

As shown in **Figure 6**, PMSQ incorporation modifies the Cp behavior of PLA. Below T_g, the biocomposites exhibit slightly higher Cp than neat PLA. Since PMSQ addition does not significantly modify T_g, the overall segmental mobility of PLA chains remains mostly unchanged. Therefore, higher Cp may be associated to localized structural rearrangements and filler–matrix interactions rather than enhanced chain mobility. In contrast, the addition of plasticizers typically reduces Cp due to increased chain mobility (Peyser, 1978).

Above the melting temperature (T_m), neat PLA exhibits higher Cp than the biocomposites. In this temperature region, crystalline domains are disrupted and enhanced segmental motion occurs, reducing the additional energy required for further temperature increase in filled systems. Furthermore, Cp gradually decreases with increasing PMSQ content. This trend can be attributed to the partial restriction of polymer chain mobility induced by the rigid filler and to the inherently lower heat capacity of PMSQ. A similar reduction in Cp following PMSQ incorporation has previously been reported for polypropylene-based composites (Mboup et al., 2025).

 doi:10.20944/preprints202605.1499.v1

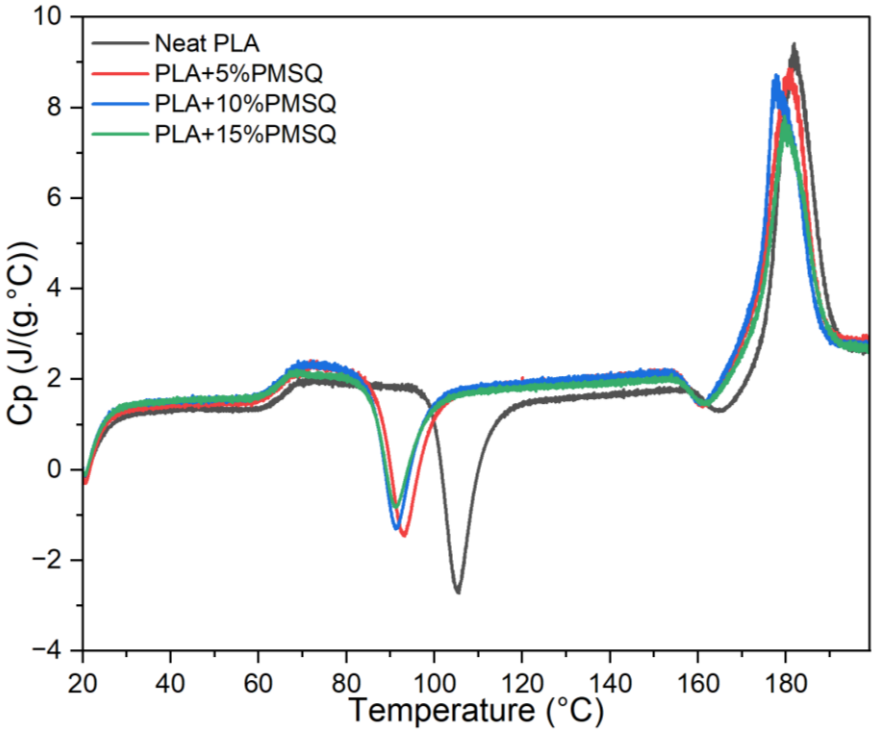

Figure 6. Heat capacity (Cp) as a function of temperature for the neat PLA and PLA/PMSQ biocomposites.

Figure 7 illustrates the thermal degradation behavior of PLA and PLA/PMSQ biocomposites, while the corresponding degradation temperatures ($T_{5\%}$, $T_{25\%}$, and $T_{50\%}$) are summarized in **Table 2**. The temperature T_{max} corresponds to the peak maximum in the differential thermogravimetry (DTG) curve.

Only minor differences in $T_{5\%}$ was observed between neat PLA and the PLA/PMSQ biocomposites, indicating that PMSQ incorporation had a limited effect on the onset of thermal degradation. However, $T_{25\%}$, $T_{50\%}$, and T_{max} slightly increased with increasing PMSQ content, suggesting a modest improvement in thermal resistance during the main degradation stage. Moreover, the residual mass continuously increased with PMSQ content. The residues increased from 4.46% for neat PLA to 7.01%, 8.00%, and 14.72% for composites containing 5, 10, and 15 wt.% PMSQ, respectively. This trend is consistent with the high thermal stability of the inorganic SiO_2 fraction of PMSQ, which does not fully decompose at 600 °C under a nitrogen atmosphere (Hedayati et al., 2020; Mboup et al., 2025). Consequently, the incorporation of PMSQ leads to enhanced thermal stability compared to neat PLA (Akindoyo et al., 2021).

Additionally, the biocomposites exhibit a distinct degradation stage between 380 and 480 °C, which is not observed in neat PLA. This additional degradation behavior may reflect a modification of the degradation kinetics of PLA resulting from PMSQ incorporation, contributing to enhanced thermal stability (Barczewski et al., 2024). While the PLA matrix undergoes thermal decomposition in this temperature range, PMSQ remains stable due to its inorganic silica-like structure. This stability may also contribute to improved flame-retardant performance of the biocomposites (Jia et al., 2019). Similar behavior has been reported for PLA reinforced with silica particles under oxidative conditions, where enhanced thermal resistance was observed (Díez-Rodríguez et al., 2020).

 doi:10.20944/preprints202605.1499.v1

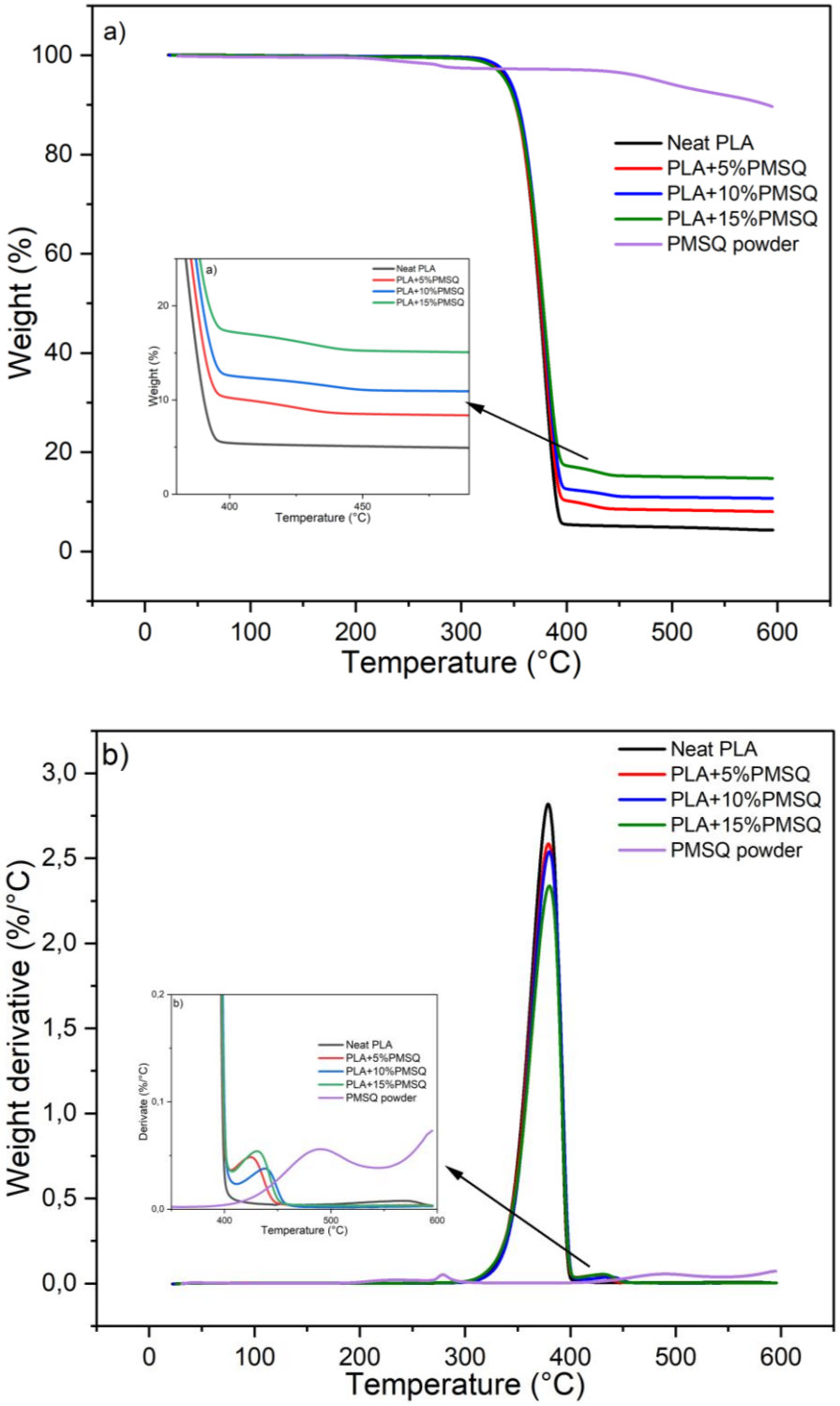

Figure 7. Thermogravimetric curves for the neat PLA and PLA/PMSQ biocomposites: a) TGA and b) DTG.

3.4. Mechanical Properties

The effect of PMSQ microparticles on the mechanical properties of PLA is presented in **Figure 8**, and the corresponding numerical values are summarized in **Table 3**. **Figure 8a** illustrates the variation in Young's modulus (E) as a function of PMSQ content. Adding 5 wt.% PMSQ did not significantly affect the Young's modulus of PLA. However, significant decreases were observed at 10 and 15 wt.% PMSQ compared with neat PLA. At 15 wt.% PMSQ, the Young's modulus decreased from 1431 MPa for neat PLA to 1300 MPa for the biocomposite, corresponding to a 9% reduction. Lower E values can be attributed to the formation of particle agglomerates and interfacial voids

 doi:10.20944/preprints202605.1499.v1

within the composite structure, as evidenced by SEM observations in **Figure 4** (Can and Kaynak, 2020; Orisekeh et al., 2025). A similar decrease in Young's modulus (10-15%) has been reported for PLA composites reinforced with POSS particles, supporting the tendency of silsesquioxane-based fillers to reduce stiffness at higher contents when interfacial interactions are limited (Sirin et al., 2016).

The incorporation of PMSQ microparticles also results in a slight reduction in yield strength (R_m) and tensile strength (R_p) at 5 and 10 wt.% content (**Figure 8b,c**). However, a more pronounced decrease (up to 20%) is observed for both parameters at 15 wt.% PMSQ. Lower yield strength may be associated with increased chain slippage in the PLA matrix, potentially facilitated by improved filler dispersion in the presence of MAPP (Sirin et al., 2016). In contrast, the reduction in tensile strength is more likely related to microstructural defects, including PMSQ agglomeration and interfacial voids, as evidenced by SEM observations in **Figure 4** (Orisekeh et al., 2025). The formation of agglomerates suggests that filler–filler interactions become dominant over matrix–filler interactions at higher concentration, resulting in weaker interfacial adhesion. Consequently, stress transfer from the matrix to the filler becomes less efficient, promoting premature failure (Haafiz et al., 2013; Mathew et al., 2005). A similar trend was reported for PLA composites reinforced with basalt particles, where a 56% reduction in tensile strength was observed at 5 wt.% (Aykanat and Ermeydan, 2022). More generally, filler contents above 5 wt.% in thermoplastic matrices tend to promote agglomeration, leading to lower tensile performance (Wen et al., 2009).

These observations were further confirmed by an analysis of variance (ANOVA). The significance of each parameter was assessed based on the *p*-value. A *p*-value lower than 0.05 indicates that the parameter under consideration has a statistically significant effect on the measured response. For the Young's modulus, a *p*-value of 0.0561 was obtained for the PLA+5%PMSQ biocomposite, indicating that the incorporation of 5 wt.% PMSQ did not significantly affect the Young's modulus of PLA. In contrast, the biocomposites containing 10 and 15 wt.% PMSQ exhibited *p*-values lower than 0.05, indicating a significant decrease in Young's modulus. A similar trend was observed for tensile strength (R_p) and yield strength (R_m). For the PLA+5%PMSQ biocomposite, *p*-values higher than 0.05 were obtained for both parameters, indicating that the addition of 5 wt.% PMSQ did not significantly affect the tensile strength or yield strength of PLA. In contrast, the biocomposites containing 10 and 15 wt.% PMSQ exhibited *p*-values lower than 0.05, revealing significant decreases in both tensile strength and yield strength at these filler contents.

The incorporation of PMSQ also resulted in lower yield strain (ε_m) and elongation at break (ε_r) (**Table 3**). This behavior is commonly observed in particle-reinforced composites and is generally attributed to the restricted mobility of polymer chains induced by the presence of rigid fillers limiting the deformability of the matrix (Bagheriasl et al., 2015; Hidalgo-Salazar and Salinas, 2019; Mustapha et al., 2022).

The progressive reduction in Young's modulus, tensile strength, and yield strength with increasing PMSQ content is mainly associated with the accumulation of microstructural defects, including interfacial voids, particle agglomeration, and restricted polymer chain mobility. These factors collectively hinder efficient stress transfer within the composite and promote premature mechanical failure.

 doi:10.20944/preprints202605.1499.v1

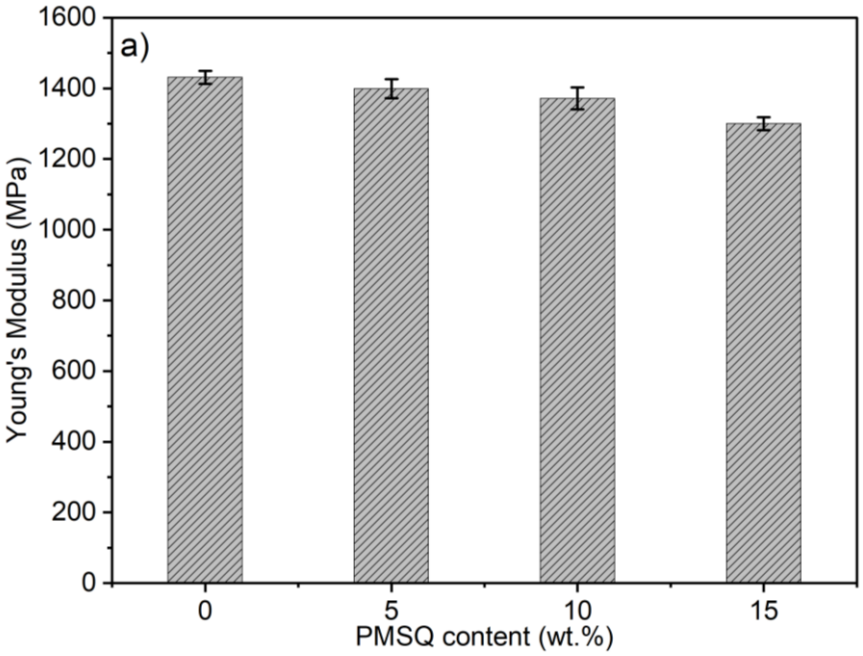

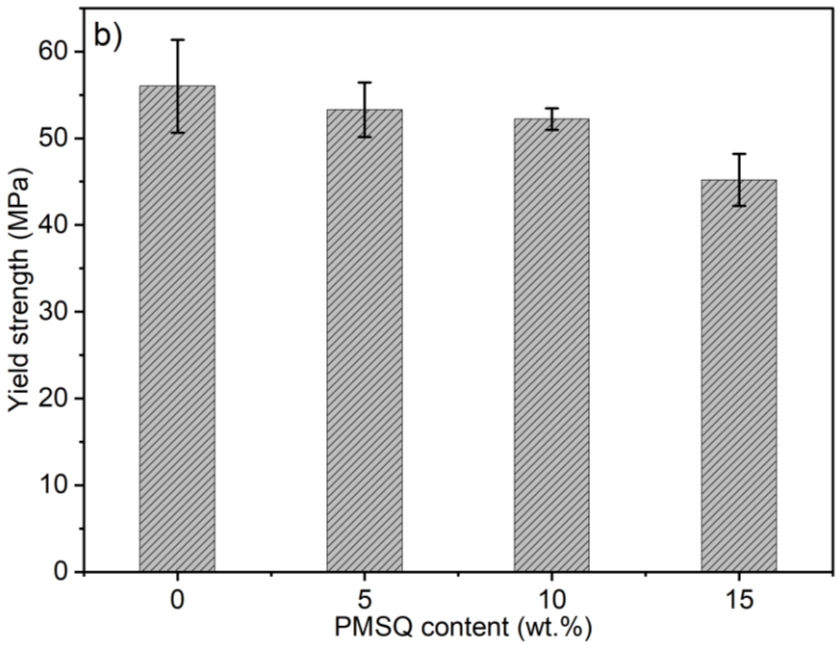

 doi:10.20944/preprints202605.1499.v1

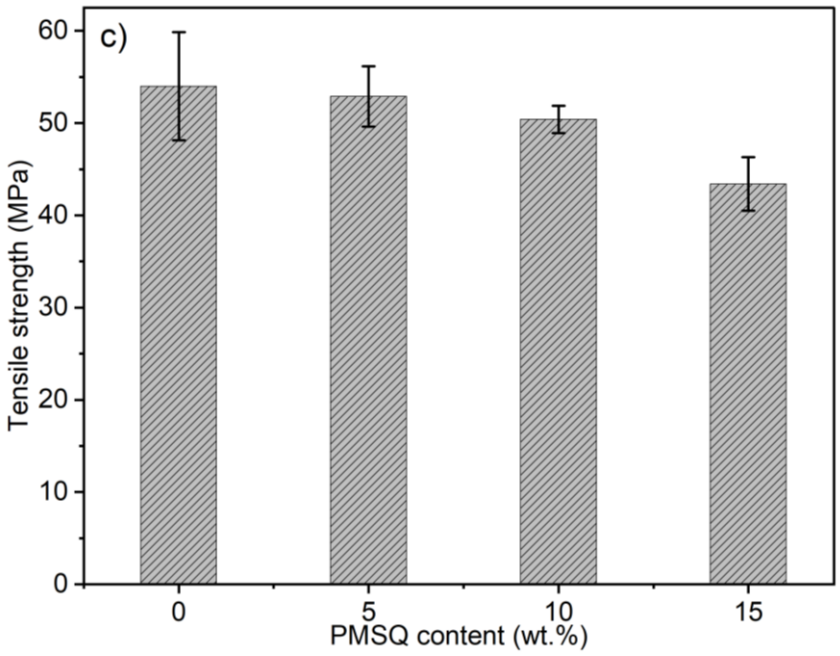

Figure 8. Tensile properties of the neat PLA and PLA/PMSQ biocomposites: a) Young's modulus; b) yield strength, and c) tensile strength.

Table 3. Mechanical properties of the neat PLA and PLA/PMSQ biocomposites.

Sample	E (MPa)	R_m (MPa)	ε_m (mm/mm)	R_p (MPa)	ε_r (mm/mm)
Neat PLA	1431±18	55.9±5.3	0.047±0.007	54.0±5.9	0.045±0.010
PLA+5%PMSQ	1399±27	53.3±3.1	0.043±0.003	52.9±3.3	0.042±0.003
PLA+10%PMSQ	1372±31	52.2±1.2	0.043±0.003	50.4±1.5	0.041±0.003
PLA+15%PMSQ	1300±18	45.2±3.0	0.038±0.003	43.4±2.9	0.036±0.002

Figure 9. presents the impact strength of the neat PLA and PLA/PMSQ biocomposites. A progressive decrease in impact resistance is observed with increasing PMSQ content. The composite containing 15 wt.% PMSQ exhibits the lowest value (21.9 J/m), corresponding to a 25% reduction relative to neat PLA (29.3 J/m). This reduction can be attributed to limited interfacial adhesion between PLA and PMSQ, especially at higher filler contents. In addition, particle agglomeration and the resulting microstructural heterogeneities act as stress concentrators, promoting crack initiation and propagation under impact loading. The impact performance of polymer composites is strongly influenced by matrix–filler interactions and the quality of interfacial bonding (Ramasamy et al., 2022). Similar trends have been reported in the literature. For instance, adding 5 wt.% eggshell microparticles in PLA led to a 24% decrease in impact strength (Orisekeh et al., 2025).

 doi:10.20944/preprints202605.1499.v1

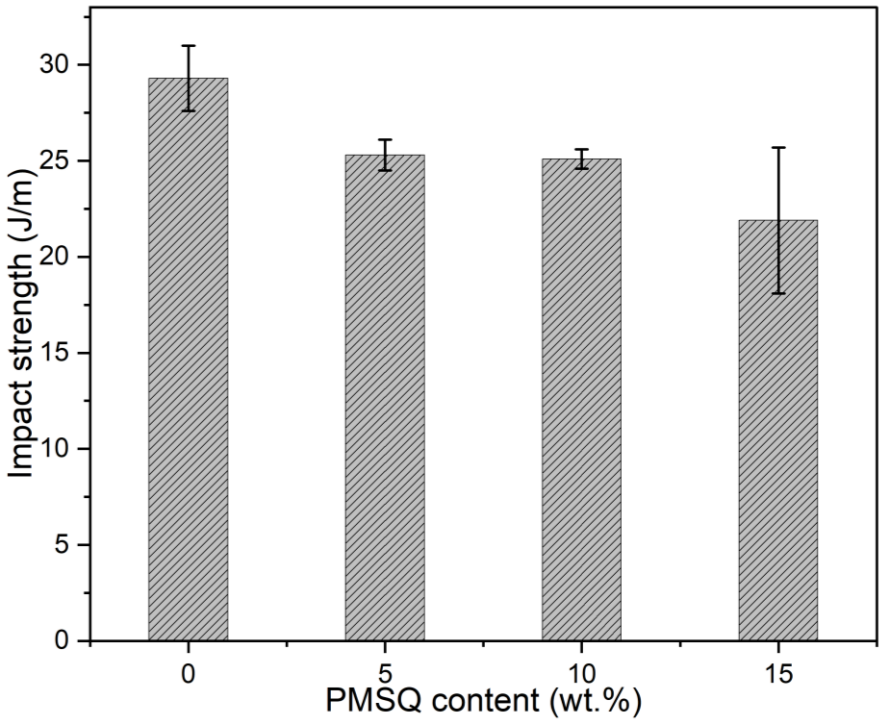

Figure 9. Impact strength of the neat PLA and PLA/PMSQ biocomposites.

3.5. Dynamic Mechanical Analysis

Figure 10 and **Table 4** present the evolution of the storage modulus (E′) as a function of temperature for the neat PLA and PLA/PMSQ biocomposites. A significant effect of PMSQ incorporation on the thermomechanical behavior is observed.

In the glassy region (30–50 °C), the biocomposite containing 5 wt.% PMSQ exhibits a higher storage modulus than neat PLA. At 35 °C, the addition of 5 wt.% PMSQ results in a 15% increase in E′. This enhancement indicates improved stiffness in the glassy state, which can be attributed to the rigid nature of PMSQ particles and their relatively uniform dispersion within the matrix. These results are consistent with SEM observations (**Figure 4**), which revealed good particle distribution at 5 wt.%, and with DSC findings (**Table 2**), which showed an increase in crystallinity at this filler concentration. The nucleating effect of PMSQ promotes higher crystalline content, thereby contributing to improved thermomechanical performance (Feng et al., 2018). Similar improvements have been reported for PLA reinforced with 5 wt.% silica particles (Fukushima et al., 2011).

In the same temperature range (30–50 °C), the biocomposites containing 10 and 15 wt.% PMSQ exhibit lower E′ values compared to neat PLA and the 5 wt.% formulation, in agreement with the tensile test results (**Figure 8**). This reduction may be associated with decreased effective crystallinity and the formation of particle agglomerates at higher filler contents (Orisekeh et al., 2025). These results suggest the existence of an optimal filler content around 5 wt.%, above which both mechanical and thermomechanical properties begin to deteriorate. A comparable trend has been reported for PLA reinforced with modified silsesquioxane nanoparticles at similar contents, where increased particle agglomeration at higher concentrations led to lower storage modulus (Barczewski et al., 2024).

In the glass transition region (50–65 °C), the composites display comparable E′ values. However, while neat PLA undergoes a pronounced reduction in stiffness near 50 °C, the PLA/PMSQ composites maintain significant rigidity up to 60 °C (**Table 4**). This shift in stiffness retention suggests enhanced thermomechanical stability resulting from PMSQ incorporation. The presence of rigid particles and increased crystallinity likely delay the softening process by restricting segmental chain mobility near the glass transition region (Barczewski et al., 2024; Orisekeh et al., 2025).

 doi:10.20944/preprints202605.1499.v1

The storage modulus (E′) obtained from DMA is systematically higher than the Young's modulus (E) measured under quasi-static conditions. This difference is mainly related to the higher oscillatory frequency and lower strain amplitude applied during DMA testing compared to static tensile experiments (Nazhat et al., 2000). Under dynamic solicitation, the restricted time available for molecular relaxation results in an apparently higher stiffness.

While quasi-static tests show a gradual decrease in Young's modulus with increasing PMSQ content, DMA reveals a more nuanced behavior. In the glassy region, the incorporation of 5 wt.% PMSQ leads to an increase in E′ compared to neat PLA. However, the storage modulus decreases at higher filler contents (10 and 15 wt.%). This improvement at low filler concentration can be attributed to uniform particle dispersion and effective stress transfer, which contribute to improved stiffness. Conversely, particle agglomeration at higher PMSQ contents weakens interfacial bonding and creates stress concentration sites, leading to reduced thermomechanical performance.

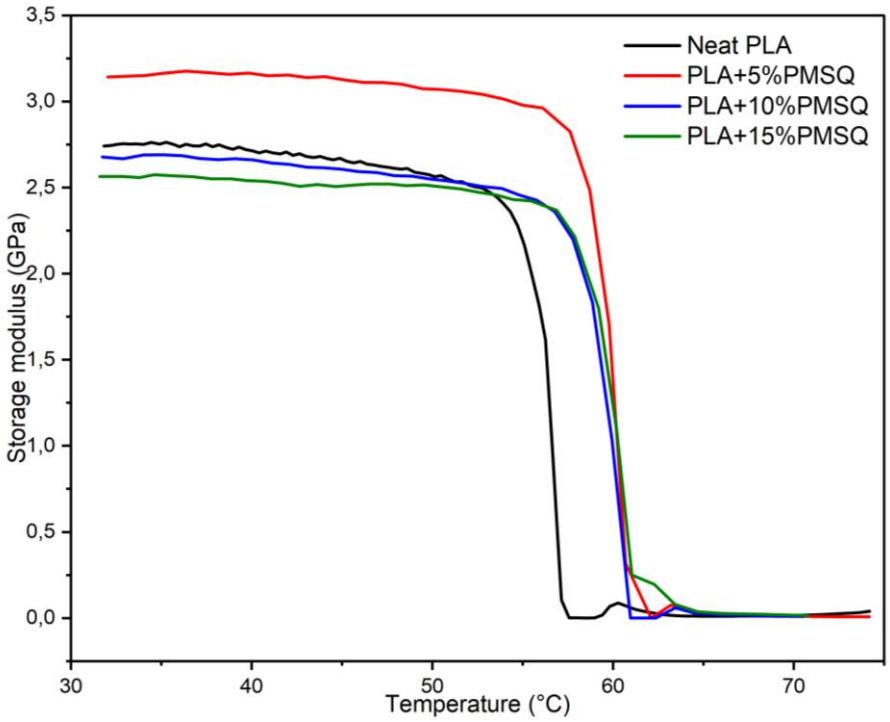

Figure 10. Storage modulus (E′) as a function of temperature for the neat PLA and PLA/PMSQ biocomposites.

Table 4. Properties obtained from DMA analysis for the neat PLA and PLA/PMSQ biocomposites.

Sample	E′ (GPa)		T_g (°C)
	At 50 °C	At 60 °C	
Neat PLA	2.56	0.09	62.5
PLA+5%PMSQ	3.07	1.71	64.6
PLA+10%PMSQ	2.55	1.03	64.5
PLA+15%PMSQ	2.52	1.09	64.7

Figure 11 presents the damping factor (tan δ) as a function of temperature for neat PLA and PLA/PMSQ biocomposites. The α-relaxation peak (Tα), corresponding to the glass transition temperature (T_g), is clearly observed. For neat PLA, T_g is located at 62.5 °C, whereas it shifts to 64.5 °C for the biocomposites (**Table 4**). This slight increase indicates a restriction of molecular mobility in the amorphous phase induced by PMSQ incorporation. The reduction in free volume resulting from filler–matrix interactions likely contributes to this shift (Baatti et al., 2020; Yu et al., 2012). In addition, the increase in crystalline content observed in DSC (**Table 2**) and the rigid nature of PMSQ

 doi:10.20944/preprints202605.1499.v1

particles dispersed in the PLA matrix further limit segmental motion, thereby enhancing the thermomechanical stability of the biocomposites (Barczewski et al., 2024).

Furthermore, a progressive decrease in the intensity of the tan δ peak (Tα) is observed for the PLA/PMSQ biocomposites. This reduction can be associated with restricted polymer chain mobility resulting from the increasing presence of rigid PMSQ microparticles (Hassan and Koyama, 2020; Orisekeh et al., 2025). A lower tan δ peak intensity generally reflects reduced molecular damping and lower chain segment mobility, which is consistent with the enhanced stiffness of the biocomposites. Incorporating PMSQ microparticles restricts internal friction mechanisms in the amorphous phase, modifying the energy dissipation behavior relative to neat PLA (Tang et al., 2012). Similar trends have been reported for PLA biocomposites reinforced with copper microparticles over a wide filler range (0–30 wt.%) (Barczewski et al., 2024).

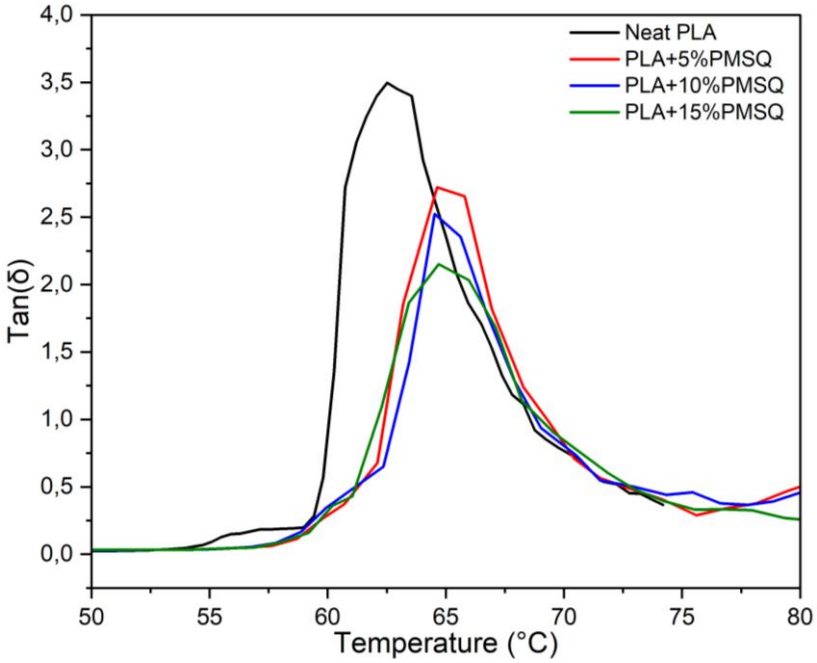

Figure 11. Tan(δ) as a function of temperature for the neat PLA and PLA/PMSQ biocomposites.

3.6. Rheological Properties

The rheological properties of neat PLA and PLA/PMSQ biocomposites were characterized by small-amplitude oscillatory shear (SAOS) at an average processing temperature of 180 °C. The dynamic storage modulus (G′) is related to the elastic behavior of the material and can be defined as the amount of energy stored. In contrast, the dynamic loss modulus (G′′) represents the amount of energy dissipated, while the complex viscosity (η*) represents the resistance to flow which is influenced by the filler shape, size, and content. These parameters provide important information on the behavior of polymeric materials in the melt state (Silva et al., 2014; Tazi et al., 2014). These parameters are discussed next.

3.6.1. Storage Modulus (G′)

The rheological curves of the samples are presented in **Figure 12** showing the behavior of typical filler-polymer composites (Park et al., 2013).

Figure 12a illustrates the effect of PMSQ incorporation on the storage modulus (G′) of PLA. For both the neat PLA and biocomposites, G′ increases with frequency over the investigated range. In addition, the incorporation of PMSQ microparticles results in a gradual increase in G′, indicating that the biocomposites exhibit higher G′ values than neat PLA. This behavior suggests that PMSQ microparticles effectively restrict the mobility of PLA chains and reinforce the elastic network within

 doi:10.20944/preprints202605.1499.v1

the matrix. It is well established that rigid fillers can form a structural network in polymer matrices, thereby limiting macromolecular chain mobility and increasing material stiffness (Wang et al., 2019). Furthermore, increasing G′ with PMSQ addition is more pronounced at low frequencies than at higher ones. This behavior may be attributed to the presence of PMSQ particles, which hinder PLA chain mobility and thus enhance the material's ability to store deformation energy (Li et al., 2016; Mohan Bhasney et al., 2020).

3.6.2. Loss Modulus (G′′)

The effect of PMSQ microparticles on the loss modulus (G′′) of the neat PLA and the biocomposites is shown in **Figure 12b**. Similar to the storage modulus (G′), the loss modulus increases over the frequency range for all materials. Furthermore, the incorporation of PMSQ results in a gradual increase in G′′ values. In other words, the biocomposites exhibit higher loss modulus values than neat PLA. This behavior suggests an enhanced ability of the biocomposites to dissipate energy (Mohan Bhasney et al., 2020), which may be attributed to restricted polymer chain mobility and stronger filler–matrix interfacial interactions promoted by the coupling agent (MAPP).

3.6.3. Complex Viscosity (η*)

Spherical particles exhibit a high viscosity threshold (50-60%), offering an advantage in the field of polymer-based composites (Chen et al., 2016).

Figure 12c shows the complex viscosity curves of the neat PLA and its biocomposites. Incorporating PMSQ microparticles leads to a gradual increase in the viscosity. This increase may be associated with the presence of the coupling agent (MAPP), which enhances interfacial interactions between the polymer matrix and the filler. These interactions restrict macromolecular mobility and increase resistance to flow, thereby leading to higher viscosity (Qiao et al., 2021). PMSQ incorporation causes an upward shift in the complex viscosity curve without significantly altering the relaxation spectrum of PLA macromolecules. This behavior is typically observed in polymer-based composites with weak polymer–filler interactions, where the dispersed particles do not significantly affect macromolecular dynamics (Arrigo et al., 2020). By comparison, Silva et al. reported a decrease in the viscosity of PLA with the addition of talc particles, which was attributed to the lubricating effect induced by the mineral filler (Silva et al., 2014).

Furthermore, neat PLA exhibits a Newtonian plateau, corresponding to the zero-shear viscosity, over the investigated frequency range. In contrast, the biocomposites display quasi-Newtonian behavior up to 10 rad/s, followed by a slight decrease in viscosity at higher frequencies due to shear-thinning behavior (De Almeida et al., 2016; Silva et al., 2014).

 doi:10.20944/preprints202605.1499.v1

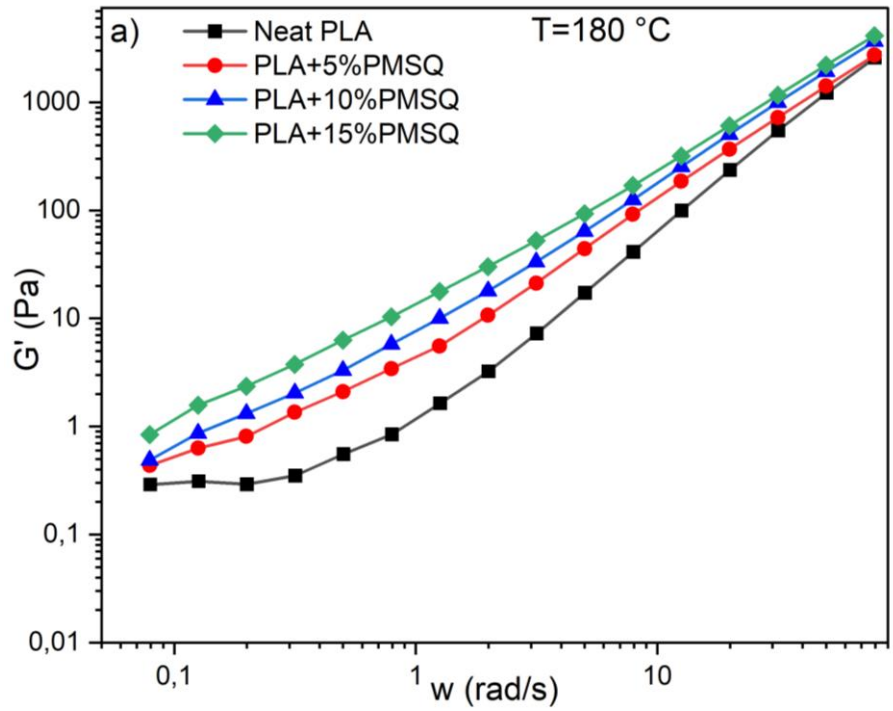

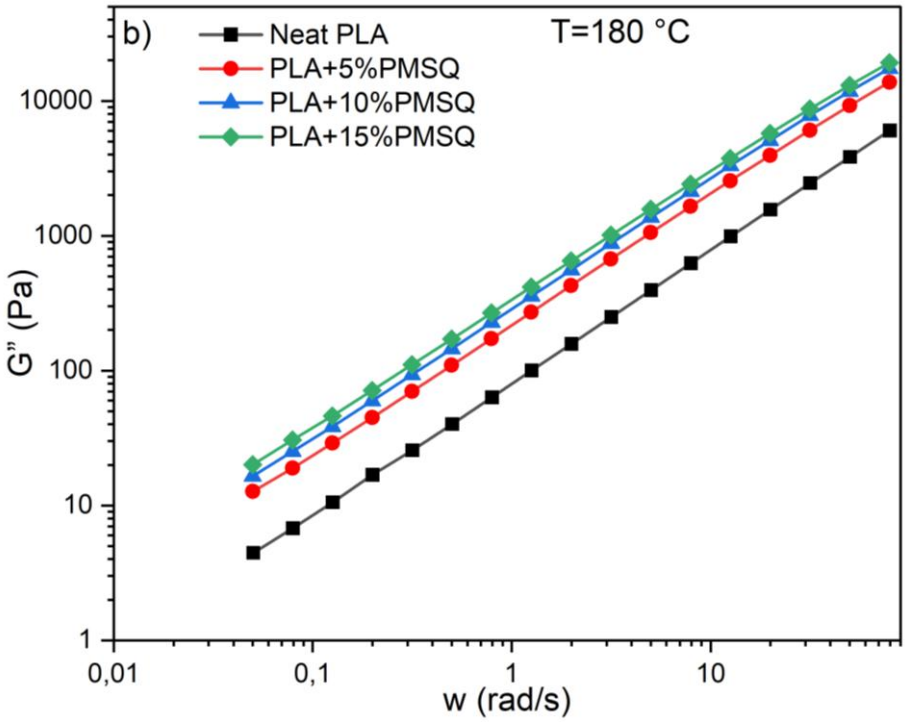

 doi:10.20944/preprints202605.1499.v1

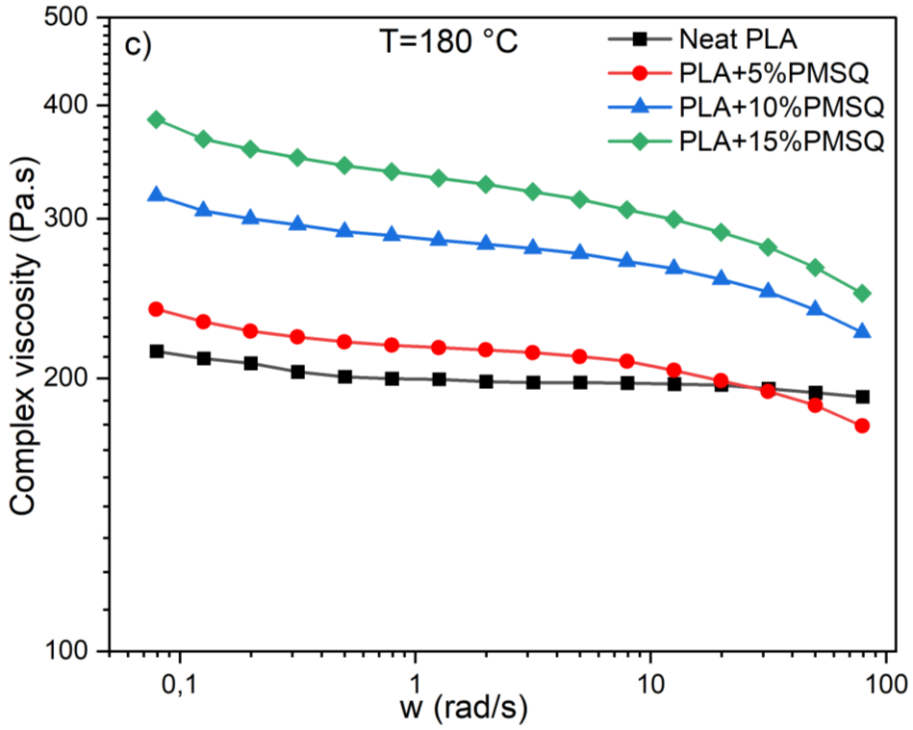

Figure 12. Rheological properties of the neat PLA and PLA/PMSQ biocomposites at 180 °C: a) storage modulus (G'), b) loss modulus (G''), and c) complex viscosity (η*).

3.7. Thermal Conductivity

Figure 13 illustrates the effect of PMSQ microparticles on the thermal conductivity of PLA measured at 23, 50, 75, and 100 °C.

Thermal conductivity increased significantly between 23 and 75 °C for all PLA/PMSQ composites. At 75 °C, the composites reached a thermal conductivity of 0.180 W/(m.K), compared with 0.146 W/(m.K) for neat PLA, corresponding to a 23% increase. This improvement can be attributed to enhanced interparticle contact between PMSQ microparticles, which facilitates phonon transport and reduces interfacial thermal resistance, thereby promoting the formation of thermally conductive pathways within the matrix (Blanco et al., 2022; Chen et al., 2016). A similar trend was reported in our previous work on PP/PMSQ composites, where the incorporation of 10 wt.% PMSQ increased the thermal conductivity by 18% (from 0.187 to 0.220 W/(m.K)) (Mboup et al., 2025). In addition, higher crystallinity observed in **Table 2** may contribute to enhanced heat transfer. Crystalline domains provide more ordered chain packing, which promotes more efficient phonon propagation compared to amorphous regions (Barkhad et al., 2020).

At higher temperature (100 °C), corresponding to conditions above T_g, the enhancement in thermal conductivity becomes less pronounced. Neat PLA exhibits a thermal conductivity of 0.221 W/(m.K), while the incorporation of 15 wt.% PMSQ increases this value to 0.233 W/(m.K), corresponding to a modest improvement of 6%. Above T_g, the polymer matrix transitions into a rubbery state characterized by increased segmental mobility and reduced structural order. The enhanced molecular motion and partial disruption of ordered domains decrease the efficiency of phonon transport inside the matrix, thereby limiting the relative contribution of PMSQ particles to overall thermal conduction. As a result, the difference in thermal conductivity between neat PLA and the biocomposites becomes less significant at elevated temperatures.

Previous studies have shown that the incorporation of thermally conductive fillers into thermoplastic matrices enhances thermal conductivity through the formation of conductive pathways, with efficiency increasing with filler concentration (Duan et al., 2012; Guo et al., 2019). Moreover, higher crystallinity reduces intermolecular spacing and promotes more compact chain packing, thereby facilitating heat transfer inside composites (Barkhad et al., 2020).

 doi:10.20944/preprints202605.1499.v1

Nevertheless, the improved thermal conductivity achieved in the present study remains significantly lower than that reported for highly conductive fillers. For instance, the incorporation of 9 wt.% graphene in PLA resulted in a 263% increase in thermal conductivity, reaching 0.725 W/(m.K), compared to 0.2 W/(m.K) for neat PLA (Spinelli et al., 2021).

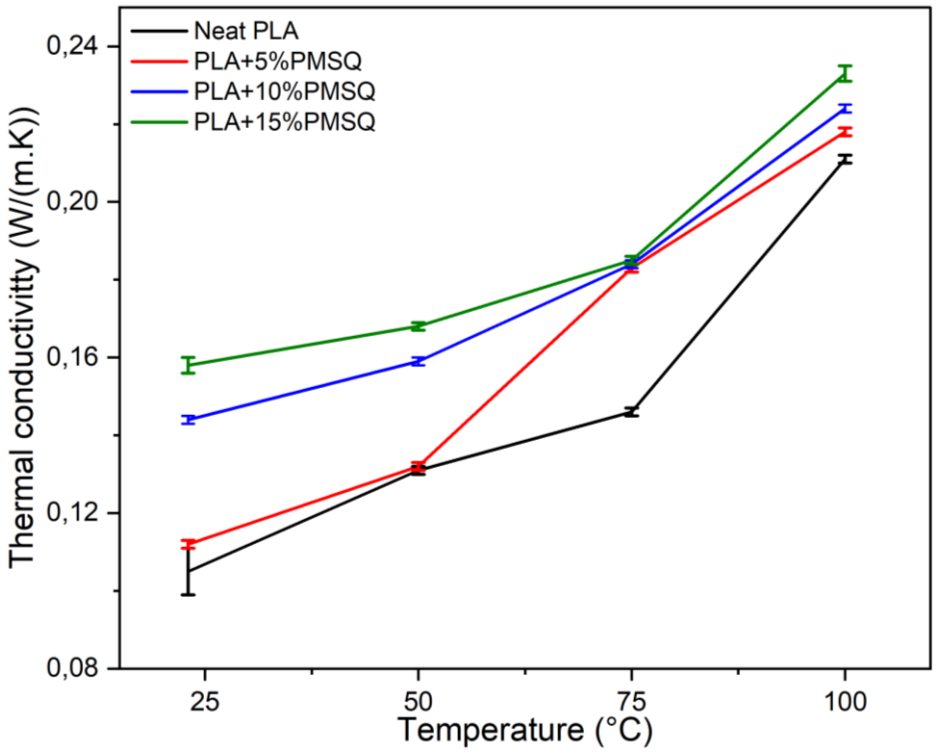

Figure 13. Thermal conductivity as a function of temperature for the neat PLA and PLA/PMSQ biocomposites.

4. Conclusion

This study investigated the effect of polymethylsilsesquioxane (PMSQ) microparticles (0–15 wt.%) on the morphological, thermal, mechanical, thermomechanical, and rheological properties of polylactic acid (PLA).

FTIR and SEM analyses confirmed the successful incorporation of PMSQ inside the PLA matrix and revealed good particle dispersion, especially at low filler content (5 wt.%). Differential scanning calorimetry (DSC) showed that the melting temperature (T_m) of PLA remained unaffected with PMSQ addition. In contrast, significant changes were observed in the cold crystallization behavior and crystallinity. The incorporation of 5 wt.% PMSQ reduced the cold crystallization temperature (T_{cc}) by 14 °C and increased the degree of crystallinity up to 100% relative to neat PLA, indicating an effective nucleating effect. Thermogravimetric analysis (TGA) revealed a slight improvement in thermal stability, as evidenced by modest increases in degradation temperatures and a progressive increase in residue with increasing PMSQ content.

Mechanical testing revealed a reduction in Young's modulus, tensile strength, and yield stress, especially at higher PMSQ concentration (10–15 wt.%). In contrast, dynamic mechanical analysis (DMA) showed that adding 5 wt.% PMSQ led to higher storage modulus (E′), with an improvement of 15% at 35 °C relative to neat PLA. But this improvement was no longer observed at higher filler contents, consistent with the formation of microstructural defects at elevated contents. In particular, the biocomposites retained their stiffness at temperatures up to 10 °C higher than neat PLA, indicating improved thermomechanical stability. DMA also revealed a slight upward shift in the glass transition temperature (T_g), reflecting restricted molecular mobility induced by PMSQ incorporation. Rheological measurements showed increased storage (G′) and loss (G′′) moduli, as well as higher complex viscosity (η^*). Thermal conductivity measurements showed a continuous

 doi:10.20944/preprints202605.1499.v1

increase over the investigated temperature range (23–100 °C). At 75 °C, the biocomposites exhibited a 23% increase compared to neat PLA, highlighting the contribution of PMSQ microparticles to improved heat transfer.

In summary, this study confirmed the possibility of developing PLA-based biocomposites incorporating PMSQ microparticles with improved thermomechanical and thermal conductivity properties. While PMSQ effectively enhanced stiffness retention and thermal conductivity, a reduction in tensile and impact performance was observed at higher filler concentration.

Future work should therefore focus on optimizing PMSQ content around 5 wt.% and improve interfacial interactions to mitigate strength loss. In addition, the development of ternary systems such as PLA/PHB/PMSQ represents a promising strategy to further tailor the balance between stiffness, toughness, and thermal performance.

These findings suggest that PLA/PMSQ biocomposites are promising candidates for infrared-assisted thermoforming applications, owing to their improved thermomechanical properties and enhanced thermal conductivity, which may promote more efficient heat transfer during heating.

Acknowledgments: The authors gratefully acknowledge the financial support provided by the Natural Sciences and Engineering Research Council of Canada (RGPIN-2016-05689), the Fondation J.A. DeSève, and the Fondation de l'UQAT. The authors also sincerely acknowledge CERMA (Research Center on Advanced Materials) at Université Laval for providing access to the facilities and instrumentation essential to this work.

References

1. Akindoyo, J.O., Beg, M.D.H., Ghazali, S., Heim, H.P., Feldmann, M., Mariatti, M., 2021. Simultaneous impact modified and chain extended glass fiber reinforced poly(lactic acid) composites: Mechanical, thermal, crystallization, and dynamic mechanical performance. J of Applied Polymer Sci 138, 49752. https://doi.org/10.1002/app.49752
2. Aliotta, L., Cinelli, P., Coltelli, M.B., Lazzeri, A., 2019. Rigid filler toughening in PLA-Calcium Carbonate composites: Effect of particle surface treatment and matrix plasticization. European Polymer Journal 113, 78–88. https://doi.org/10.1016/j.eurpolymj.2018.12.042
3. Anjrini, N., Karabulut, H., Ulag, S., Ege, H., Noberi, C., Dogan, E., Sahin, A., Gunduz, O., 2024. 3D-printed polylactic acid (PLA)/polymethyl silsesquioxane (PMSQ)-based scaffolds coated with vitamin E microparticles for the application of wound healing. emergent mater. 7, 2595–2604. https://doi.org/10.1007/s42247-024-00711-3
4. Arrigo, R., Bartoli, M., Malucelli, G., 2020. Poly(lactic Acid)–Biochar Biocomposites: Effect of Processing and Filler Content on Rheological, Thermal, and Mechanical Properties. Polymers 12, 892. https://doi.org/10.3390/polym12040892
5. Awal, A., Rana, M., Sain, M., 2015. Thermorheological and mechanical properties of cellulose reinforced PLA bio-composites. Mechanics of Materials 80, 87–95. https://doi.org/10.1016/j.mechmat.2014.09.009
6. Aykanat, O., Ermeydan, M.A., 2022. Production of basalt/wood fiber reinforced polylactic acid hybrid biocomposites and investigation of performance features including insulation properties. Polymer Composites 43, 3519–3530. https://doi.org/10.1002/pc.26633
7. Baatti, A., Erchiqui, F., Godard, F., Bussières, D., Bébin, P., 2020. DMA analysis, thermal study and morphology of polymethylsilsesquioxane nanoparticles-reinforced HDPE nanocomposite. J Therm Anal Calorim 139, 789–797. https://doi.org/10.1007/s10973-019-08497-x
8. Bagheriasl, D., Carreau, P.J., Dubois, C., Riedl, B., 2015. Effect of cellulose nanocrystals (CNCs) on crystallinity, mechanical and rheological properties of polypropylene/CNCs nanocomposites. Presented at the PROCEEDINGS OF PPS-30: The 30th International Conference of the Polymer Processing Society – Conference Papers, Cleveland, Ohio, USA, p. 070010. https://doi.org/10.1063/1.4918445
9. Barczewski, M., Paszkiewicz, S., Cañavate, J., Aniśko, J., Hejna, A., Piasecki, A., Dudziec, B., 2024. Crystallization behavior and thermal properties of octa-phenyl-substituted silsesquioxane-modified polylactide (PLA). J Mater Sci 59, 20445–20461. https://doi.org/10.1007/s10853-024-10328-w

 doi:10.20944/preprints202605.1499.v1

10. Barkhad, M.S., Abu-Jdayil, B., Mourad, A.H.I., Iqbal, M.Z., 2020. Thermal Insulation and Mechanical Properties of Polylactic Acid (PLA) at Different Processing Conditions. Polymers 12, 2091. https://doi.org/10.3390/polym12092091
11. Blanco, I., Cicala, G., Recca, G., Tosto, C., 2022. Specific Heat Capacity and Thermal Conductivity Measurements of PLA-Based 3D-Printed Parts with Milled Carbon Fiber Reinforcement. Entropy 24, 654. https://doi.org/10.3390/e24050654
12. Can, U., Kaynak, C., 2020. Effects of micro-nano titania contents and maleic anhydride compatibilization on the mechanical performance of polylactide. Polymer Composites 41, 600–613. https://doi.org/10.1002/pc.25391
13. Chang, Z., Lei, L., Zhu, L., Quan, Y., Ren, Z., Qian, Y., Dastan, D., Shi, Z., 2025. Remarkably boosted high-temperature energy storage of a polymer dielectric induced by polymethylsesquioxane microspheres. Materials Horizons.
14. Chen, H., Ginzburg, V.V., Yang, J., Yang, Y., Liu, W., Huang, Y., Du, L., Chen, B., 2016. Thermal conductivity of polymer-based composites: Fundamentals and applications. Progress in Polymer Science 59, 41–85. https://doi.org/10.1016/j.progpolymsci.2016.03.001
15. Cristea, M., Ionita, D., Iftime, M.M., 2020. Dynamic Mechanical Analysis Investigations of PLA-Based Renewable Materials: How Are They Useful? Materials 13, 5302. https://doi.org/10.3390/ma13225302
16. D'Anna, A., Arrigo, R., Frache, A., 2022. Rheology, Morphology and Thermal Properties of a PLA/PHB/Clay Blend Nanocomposite: The Influence of Process Parameters. J Polym Environ 30, 102–113. https://doi.org/10.1007/s10924-021-02186-3
17. D'Anna, A., Arrigo, R., Frache, A., 2019. PLA/PHB Blends: Biocompatibilizer Effects. Polymers 11, 1416. https://doi.org/10.3390/polym11091416
18. De Almeida, J.F.M., Da Silva, A.L.N., Escócio, V.A., Da Fonseca Thomé Da Silva, A.H.M., De Sousa, A.M.F., Nascimento, C.R., Bertolino, L.C., 2016. Rheological, mechanical and morphological behavior of polylactide/nano-sized calcium carbonate composites. Polym. Bull. 73, 3531–3545. https://doi.org/10.1007/s00289-016-1656-9
19. Díez-Rodríguez, T.M., Blázquez-Blázquez, E., Pérez, E., Cerrada, M.L., 2020. Composites Based on Poly(Lactic Acid) (PLA) and SBA-15: Effect of Mesoporous Silica on Thermal Stability and on Isothermal Crystallization from Either Glass or Molten State. Polymers 12, 2743. https://doi.org/10.3390/polym12112743
20. Donmez, S., Tuzenli, Z., Bayram, G., Savaskan Yilmaz, S., 2024. Flame retardancy and mechanical properties of polypropylene composites containing intumescent flame retardants, preceramic polymers, and other additives. SPE Polymers 5, 318–330. https://doi.org/10.1002/pls2.10126
21. Duan, J., Shao, S., Ya-Li, Wang, L., Jiang, P., Liu, B., 2012. Polylactide/graphite nanosheets/MWCNTs nanocomposites with enhanced mechanical, thermal and electrical properties. Iran Polym J 21, 109–120. https://doi.org/10.1007/s13726-011-0008-8
22. Feng, Y., Ma, P., Xu, P., Wang, R., Dong, W., Chen, M., Joziasse, C., 2018. The crystallization behavior of poly(lactic acid) with different types of nucleating agents. International Journal of Biological Macromolecules 106, 955–962. https://doi.org/10.1016/j.ijbiomac.2017.08.095
23. Fischer, E.W., Sterzel, H.J., Wegner, G., 1973. Investigation of the structure of solution grown crystals of lactide copolymers by means of chemical reactions. Kolloid-Z.u.Z.Polymere 251, 980–990. https://doi.org/10.1007/BF01498927
24. Fukushima, K., Tabuani, D., Abbate, C., Arena, M., Rizzarelli, P., 2011. Preparation, characterization and biodegradation of biopolymer nanocomposites based on fumed silica. European Polymer Journal 47, 139–152. https://doi.org/10.1016/j.eurpolymj.2010.10.027
25. Guo, R., Ren, Z., Bi, H., Xu, M., Cai, L., 2019. Electrical and Thermal Conductivity of Polylactic Acid (PLA)-Based Biocomposites by Incorporation of Nano-Graphite Fabricated with Fused Deposition Modeling. Polymers 11, 549. https://doi.org/10.3390/polym11030549
26. Guo, Z., Shi, X., 2011. Temperature–Time Curve of Fire and the Equation of Heat Conduction, in: Experiment and Calculation of Reinforced Concrete at Elevated Temperatures. Elsevier, pp. 76–90. https://doi.org/10.1016/B978-0-12-386962-3.10005-1

 doi:10.20944/preprints202605.1499.v1

27. Gupta, A.P., Kumar, V., 2007. New emerging trends in synthetic biodegradable polymers – Polylactide: A critique. European Polymer Journal 43, 4053–4074. https://doi.org/10.1016/j.eurpolymj.2007.06.045
28. Haafiz, M.K.M., Hassan, A., Zakaria, Z., Inuwa, I.M., Islam, M.S., Jawaid, M., 2013. Properties of polylactic acid composites reinforced with oil palm biomass microcrystalline cellulose. Carbohydrate Polymers 98, 139–145. https://doi.org/10.1016/j.carbpol.2013.05.069
29. Hassan, M.M., Koyama, K., 2020. Thermomechanical and viscoelastic properties of green composites of PLA using chitin micro-particles as fillers. J Polym Res 27, 27. https://doi.org/10.1007/s10965-019-1991-2
30. Hedayati, F., Moshiri-Gomchi, N., Assaran-Ghomi, M., Sabahi, S., Bahri-Laleh, N., Mehdipour-Ataei, S., Mokhtari-Aliabad, J., Mirmohammadi, S.A., 2020. Preparation and properties of enhanced nanocomposites based on PLA/PC blends reinforced with silica nanoparticles. Polymers for Advanced Techs 31, 566–573. https://doi.org/10.1002/pat.4797
31. Hidalgo-Salazar, M.A., Salinas, E., 2019. Mechanical, thermal, viscoelastic performance and product application of PP- rice husk Colombian biocomposites. Composites Part B: Engineering 176, 107135. https://doi.org/10.1016/j.compositesb.2019.107135
32. Jandas, P.J., Mohanty, S., Nayak, S.K., 2014. Morphology and Thermal Properties of Renewable Resource-Based Polymer Blend Nanocomposites Influenced by a Reactive Compatibilizer. ACS Sustainable Chem. Eng. 2, 377–386. https://doi.org/10.1021/sc400395s
33. Jia, L., Tong, B., Li, D., Zhang, W., Yang, R., 2019. Crystallization and flame-retardant properties of polylactic acid composites with polyhedral octaphenyl silsesquioxane. Polymers for Advanced Techs 30, 648–665. https://doi.org/10.1002/pat.4501
34. Jiang, L., Zhang, J., Wolcott, M.P., 2007. Comparison of polylactide/nano-sized calcium carbonate and polylactide/montmorillonite composites: Reinforcing effects and toughening mechanisms. Polymer 48, 7632–7644. https://doi.org/10.1016/j.polymer.2007.11.001
35. Kaynak, C., Erdogan, A.R., 2016. Mechanical and thermal properties of polylactide/talc microcomposites: before and after accelerated weathering: Polylactide/Talc Microcomposites: Before and After Accelerated Weathering. Polym. Adv. Technol. 27, 812–822. https://doi.org/10.1002/pat.3721
36. Kaynak, C., Meyva, Y., 2014. Use of maleic anhydride compatibilization to improve toughness and other properties of polylactide blended with thermoplastic elastomers: Maleic Anhydride Compatibilization For Toughening Of Pla Blends. Polym. Adv. Technol. 25, 1622–1632. https://doi.org/10.1002/pat.3415
37. Kim, T.-W., Lee, S.-Y., Chun, S.-J., Doh, G.-H., Paik, K.-H., 2011. Effect of silane coupling on the fundamental properties of wood flour reinforced polypropylene composites. Journal of Composite Materials 45, 1595–1605. https://doi.org/10.1177/0021998310385589
38. Lecoublet, M., Ragoubi, M., Leblanc, N., Koubaa, A., 2024. Sustainable 3D-printed cellulose-based biocomposites and bio-nano-composites: Analysis of dielectric performances. Industrial Crops and Products 221, 119332. https://doi.org/10.1016/j.indcrop.2024.119332
39. Lee, T.-W., Jeong, Y.G., 2014. Enhanced electrical conductivity, mechanical modulus, and thermal stability of immiscible polylactide/polypropylene blends by the selective localization of multi-walled carbon nanotubes. Composites Science and Technology 103, 78–84. https://doi.org/10.1016/j.compscitech.2014.08.019
40. Li, H., Cao, Z., Wu, D., Tao, G., Zhong, W., Zhu, H., Qiu, P., Liu, C., 2016. Crystallisation, mechanical properties and rheological behaviour of PLA composites reinforced by surface modified microcrystalline cellulose. Plastics, Rubber and Composites 45, 181–187. https://doi.org/10.1179/1743289815Y.0000000040
41. Madhavan Nampoothiri, K., Nair, N.R., John, R.P., 2010. An overview of the recent developments in polylactide (PLA) research. Bioresource Technology 101, 8493–8501. https://doi.org/10.1016/j.biortech.2010.05.092
42. Mathew, A.P., Oksman, K., Sain, M., 2005. Mechanical properties of biodegradable composites from poly lactic acid (PLA) and microcrystalline cellulose (MCC). J of Applied Polymer Sci 97, 2014–2025. https://doi.org/10.1002/app.21779
43. Mboup, K., Erchiqui, F., Ben Hamou, K., Baatti, A., Rodrigue, D., 2025. Thermally conductive and electrically insulative polypropylene composites based on polymethylsilsesquioxane microparticles.

 doi:10.20944/preprints202605.1499.v1

Journal of Thermoplastic Composite Materials 08927057251371578. https://doi.org/10.1177/08927057251371578

44. Meng, G., Li, Y., Wang, Z., Pan, C., Gao, W., Cheng, Y., 2021. Preparation and Characterization of Narrow Size Distribution PMSQ Microspheres for High-Frequency Electronic Packaging. Materials 14, 4233. https://doi.org/10.3390/ma14154233
45. Mohan Bhasney, S., Kumar, A., Katiyar, V., 2020. Microcrystalline cellulose, polylactic acid and polypropylene biocomposites and its morphological, mechanical, thermal and rheological properties. Composites Part B: Engineering 184, 107717. https://doi.org/10.1016/j.compositesb.2019.107717
46. Moliner, C., Finocchio, E., Arato, E., Ramis, G., Lagazzo, A., 2020. Influence of the Degradation Medium on Water Uptake, Morphology, and Chemical Structure of Poly(Lactic Acid)-Sisal Bio-Composites. Materials 13, 3974. https://doi.org/10.3390/ma13183974
47. Mustapha, S., Lease, J., Eksiler, K., Sim, S.T., Ariffin, H., Andou, Y., 2022. Facile Preparation of Cellulose Fiber Reinforced Polypropylene Using Hybrid Filler Method. Polymers 14, 1630. https://doi.org/10.3390/polym14081630
48. Nazhat, S.N., Joseph, R., Wang, M., Smith, R., Tanner, K.E., Bonfield, W., 2000. Dynamic mechanical characterization of hydroxyapatite reinforced polyethylene: effect of particle size. Journal of Materials Science: Materials in Medicine 11, 621–628. https://doi.org/10.1023/A:1008957729512
49. Neoh, K.W., Tshai, K.Y., Khiew, P.S., Chia, C.H., 2011. Micro Palm and Kenaf Fibers Reinforced PLA Composite: Effect of Volume Fraction on Tensile Strength. AMM 145, 1–5. https://doi.org/10.4028/www.scientific.net/AMM.145.1
50. Orisekeh, D.K., Corti, G., Jahan, M.P., 2025. Enhancing thermo-mechanical properties of additively manufactured PLA using eggshell microparticle fillers. Journal of Manufacturing Processes 133, 782–797. https://doi.org/10.1016/j.jmapro.2024.11.095
51. Oseh, J.O., Mohd Norddin, M.N.A., Ismail, I., Gbadamosi, A.O., Agi, A., Mohammed, H.N., 2019. A novel approach to enhance rheological and filtration properties of water–based mud using polypropylene–silica nanocomposite. Journal of Petroleum Science and Engineering 181, 106264. https://doi.org/10.1016/j.petrol.2019.106264
52. Park, S.H., Lee, S.G., Kim, S.H., 2013. Isothermal crystallization behavior and mechanical properties of polylactide/carbon nanotube nanocomposites. Composites Part A: Applied Science and Manufacturing 46, 11–18. https://doi.org/10.1016/j.compositesa.2012.10.011
53. Peyser, P., 1978. The Effect of Fillers on Polymer Properties. Polymer-Plastics Technology and Engineering 10, 117–129. https://doi.org/10.1080/03602557809409224
54. Pyda, M., Bopp, R.C., Wunderlich, B., 2004. Heat capacity of poly(lactic acid). The Journal of Chemical Thermodynamics 36, 731–742. https://doi.org/10.1016/j.jct.2004.05.003
55. Qiao, Y., Li, Q., Jalali, A., Yang, J., Wang, X., Zhao, N., Jiang, Y., Wang, S., Hou, J., Jiang, J., 2021. In-situ microfibrillated Poly(ε-caprolactone)/ Poly(lactic acid) composites with enhanced rheological properties, crystallization kinetics and foaming ability. Composites Part B: Engineering 208, 108594. https://doi.org/10.1016/j.compositesb.2020.108594
56. Ramasamy, N., Arumugam, V., Kumar, S.C., 2022. Characterization of fiber/matrix interfacial bonding strength of chemically grafted aramid fiber surface with epoxy resin composites. Polymer Composites 43, 399–410.
57. Rao, J., Zhou, Y., Fan, M., 2018. Revealing the Interface Structure and Bonding Mechanism of Coupling Agent Treated WPC. Polymers 10, 266. https://doi.org/10.3390/polym10030266
58. Rbihi, Z., Erchiqui, F., Rodrigue, D., Kaddami, H., 2025. Thermal, Mechanical, and Rheological Properties of PLA/PHB Biocomposites Reinforced with Alkaline-Treated Hemp Fibers and Granules. ChemEngineering 9, 122. https://doi.org/10.3390/chemengineering9060122
59. Silva, A.L.N., Cipriano, T.F., ASilva, N.H.M.D.F.T.D., Rocha, M.C.C.G., Sousa, A.F., Silva, G.M.D., 2014. Thermal, rheological and morphological properties of poly (lactic acid) (PLA) and talc composites. Polímeros 24, 276–282. https://doi.org/10.4322/polimeros.2014.067
60. Sirin, H., Kodal, M., Ozkoc, G., 2016. The influence of POSS type on the properties of PLA. Polymer Composites 37, 1497–1506. https://doi.org/10.1002/pc.23319

 doi:10.20944/preprints202605.1499.v1

61. Soudmand, B.H., Shelesh-Nezhad, K., Salimi, Y., 2020. A combined differential scanning calorimetry-dynamic mechanical thermal analysis approach for the estimation of constrained phases in thermoplastic polymer nanocomposites. J of Applied Polymer Sci 137, 49260. https://doi.org/10.1002/app.49260
62. Spinelli, G., Guarini, R., Kotsilkova, R., Ivanov, E., Romano, V., 2021. Experimental, Theoretical and Simulation Studies on the Thermal Behavior of PLA-Based Nanocomposites Reinforced with Different Carbonaceous Fillers. Nanomaterials 11, 1511. https://doi.org/10.3390/nano11061511
63. Swetha, T.A., Ananthi, V., Bora, A., Sengottuvelan, N., Ponnuchamy, K., Muthusamy, G., Arun, A., 2023. A review on biodegradable polylactic acid (PLA) production from fermentative food waste - Its applications and degradation. International Journal of Biological Macromolecules 234, 123703. https://doi.org/10.1016/j.ijbiomac.2023.123703
64. Tang, G., Wang, X., Xing, W., Zhang, P., Wang, B., Hong, N., Yang, W., Hu, Y., Song, L., 2012. Thermal Degradation and Flame Retardance of Biobased Polylactide Composites Based on Aluminum Hypophosphite. Ind. Eng. Chem. Res. 51, 12009–12016. https://doi.org/10.1021/ie3008133
65. Tazi, M., Erchiqui, F., Godard, F., Kaddami, H., Ajji, A., 2014. Characterization of rheological and thermophysical properties of HDPE–wood composite. J of Applied Polymer Sci 131, app.40495. https://doi.org/10.1002/app.40495
66. Tong, X.C., 2011. Advanced Materials for Thermal Management of Electronic Packaging, Springer Series in Advanced Microelectronics. Springer New York, New York, NY. https://doi.org/10.1007/978-1-4419-7759-5
67. Wang, K., Li, T., Xie, S., Wu, X., Huang, W., Tian, Q., Tu, C., Yan, W., 2019. Influence of Organo-Sepiolite on the Morphological, Mechanical, and Rheological Properties of PP/ABS Blends. Polymers 11, 1493. https://doi.org/10.3390/polym11091493
68. Wen, X., Lin, Y., Han, C., Zhang, K., Ran, X., Li, Y., Dong, L., 2009. Thermomechanical and optical properties of biodegradable poly(L -lactide)/silica nanocomposites by melt compounding. J of Applied Polymer Sci 114, 3379–3388. https://doi.org/10.1002/app.30896
69. Yao, B., Zhang, X., Yang, F., Li, C., Sun, G., Zhang, G., Mu, Z., 2018. Morphology-controlled synthesis of polymethylsilsesquioxane (PMSQ) microsphere and its applications in enhancing the thermal properties and flow improving ability of ethylene-vinyl acetate copolymer. Powder Technology 329, 137–148. https://doi.org/10.1016/j.powtec.2018.01.074
70. Yu, F., Liu, T., Zhao, X., Yu, X., Lu, A., Wang, J., 2012. Effects of talc on the mechanical and thermal properties of polylactide. J of Applied Polymer Sci 125. https://doi.org/10.1002/app.36260